




Interaction of the Ankyrin H Core Effector of *Legionella* with the Host LARP7 Component of the 7SK snRNP Complex

Juanita Von Dwingelo,^a Ivy Yeuk Wah Chung,^b Christopher T. Price,^a Lei Li,^b Snake Jones,^a  Miroslaw Cygler,^{b,c} Yousef Abu Kwaik^{a,d}

^aDepartment of Microbiology and Immunology, University of Louisville, Louisville, Kentucky, USA

^bDepartment of Biochemistry, University of Saskatchewan, Saskatoon, Saskatchewan, Canada

^cDepartment of Biochemistry, McGill University, Montreal, Quebec, Canada

^dCenter for Predictive Medicine, College of Medicine, University of Louisville, Louisville, Kentucky, USA

ABSTRACT Species of the *Legionella* genus encode at least 18,000 effector proteins that are translocated through the Dot/Icm type IVB translocation system into macrophages and protist hosts to enable intracellular growth. Eight effectors, including ankyrin H (AnkH), are common to all *Legionella* species. The AnkH effector is also present in *Coxiella* and *Rickettsiella*. To date, no pathogenic effectors have ever been described that directly interfere with host cell transcription. We determined that the host nuclear protein La-related protein 7 (LARP7), which is a component of the 7SK small nuclear ribonucleoprotein (snRNP) complex, interacts with AnkH in the host cell nucleus. The AnkH-LARP7 interaction partially impedes interactions of the 7SK snRNP components with LARP7, interfering with transcriptional elongation by polymerase (Pol) II. Consistent with that, our data show AnkH-dependent global reprogramming of transcription of macrophages infected by *Legionella pneumophila*. The crystal structure of AnkH shows that it contains four N-terminal ankyrin repeats, followed by a cysteine protease-like domain and an α -helical C-terminal domain. A substitution within the β -hairpin loop of the third ankyrin repeat results in diminishment of LARP7-AnkH interactions and phenocopies the *ankH* null mutant defect in intracellular growth. LARP7 knockdown partially suppresses intracellular proliferation of wild-type (WT) bacteria and increases the severity of the defect of the Δ *ankH* mutant, indicating a role for LARP7 in permissiveness of host cells to intracellular bacterial infection. We conclude that the AnkH-LARP7 interaction impedes interaction of LARP7 with 7SK snRNP, which would block transcriptional elongation by Pol II, leading to host global transcriptional reprogramming and permissiveness to *L. pneumophila*.

IMPORTANCE For intracellular pathogens to thrive in host cells, an environment that supports survival and replication needs to be established. *L. pneumophila* accomplishes this through the activity of the ~330 effector proteins that are injected into host cells during infection. Effector functions range from hijacking host trafficking pathways to altering host cell machinery, resulting in altered cell biology and innate immunity. One such pathway is the host protein synthesis pathway. Five *L. pneumophila* effectors have been identified that alter host cell translation, and 2 effectors have been identified that indirectly affect host cell transcription. No pathogenic effectors have been described that directly interfere with host cell transcription. Here we show a direct interaction of the AnkH effector with a host cell transcription complex involved in transcriptional elongation. We identify a novel process by which AnkH interferes with host transcriptional elongation through interference with formation of a functional complex and show that this interference is required for pathogen proliferation.

Citation Von Dwingelo J, Chung IYW, Price CT, Li L, Jones S, Cygler M, Abu Kwaik Y. 2019. Interaction of the ankyrin H core effector of *Legionella* with the host LARP7 component of the 7SK snRNP complex. mBio 10:e01942-19. <https://doi.org/10.1128/mBio.01942-19>.

Editor Scot P. Ouellette, University of Nebraska Medical Center

Copyright © 2019 Von Dwingelo et al. This is an open-access article distributed under the terms of the [Creative Commons Attribution 4.0 International license](https://creativecommons.org/licenses/by/4.0/).

Address correspondence to Miroslaw Cygler, miroslaw.cygler@usask.ca, or Yousef Abu Kwaik, abukwaik@louisville.edu.

J.V.D. and I.Y.W.C. contributed equally to this article.

This article is a direct contribution from a Fellow of the American Academy of Microbiology. Solicited external reviewers: Michael Steinert, Technische Universität Braunschweig; Nicholas Cianciotto, Northwestern University Medical School; Amal Amer, Ohio State University; Ralph Isberg, Tufts Medical School.

Received 24 July 2019

Accepted 26 July 2019

Published 27 August 2019

KEYWORDS AnkH, Dot/Icm type IVB secretion system, LARP7, *Legionella pneumophila*, effector functions, transcriptional regulation

Legionella pneumophila is a Gram-negative intracellular pathogen that is ubiquitous in freshwater environments (1), where it primarily parasitizes a wide range of protozoan hosts, which serve as the bacterial natural hosts (2–5) and contribute to the pathogenesis and ecology of the pathogen (6–10). When humans encounter contaminated water sources, aerosolized water droplets can be inhaled and reach the lung, where bacteria can invade and proliferate within alveolar macrophages, causing pneumonia (1, 10). To date, approximately 65 species of *Legionella* have been identified, with almost half of the species having been found to be capable of causing disease in humans (11–14). *L. pneumophila* in particular is responsible for 90% of Legionnaires' disease cases globally (15).

The life cycles of *L. pneumophila* within amoebae and within alveolar macrophages are strikingly similar (5, 16–20). After the bacteria are engulfed by the cell, endoplasmic reticulum (ER)-derived vesicles fuse to the phagosome to generate the *Legionella*-containing vacuole (LCV) (18–23), which evades the host endosomal-lysosomal degradation pathway but communicates with early secretory vesicle trafficking pathways (24, 25). Biogenesis of the LCV is dependent on the Dot/Icm type IV secretion system (T4SS), which is responsible for translocation of at least 330 effector proteins into the host cell cytoplasm (26, 27). The injected effectors interact with specific host targets to modulate a plethora of host cell processes that remodel the macrophage and amoeba host into a proliferative niche (26, 28–30). In most cases, the deletion of a single *L. pneumophila* effector gene does not result in a growth defect in mammalian macrophages or amoeba (31). Although this is thought to be due to redundancy, it is more likely that many of the effectors in this arsenal are host specific and constitute a “toolbox” and that specific tools are utilized in specific environmental eukaryotic hosts (24, 32). Genomic analyses of 58 *Legionella* species have shown that the *Legionella* genus has ~18,000 effectors but that only 8 of these effectors (MavN, VipF, RavC, CetLp1, lpg2832, lpg3000, lpg1356/lpp1310, and AnkH/LegA3/Lpg2300) are conserved among all *Legionella* species and are designated core effectors (12, 14). Among the 8 core effectors, AnkH is the only one that is conserved among all bacterial pathogens harboring the Dot/Icm T4SS, including *Coxiella burnetii* and *Rickettsiella grylli* (12, 14). It is therefore likely that AnkH is involved in altering an evolutionarily conserved eukaryotic process required for the infection by many obligate and facultative intracellular pathogens.

A large number of the Dot/Icm-translocated effector proteins contain eukaryote-like motifs and domains, which is likely the result of long-term coevolution of *L. pneumophila* with its various protozoan hosts, leading to interkingdom horizontal gene transfer (9, 32–37). Examples of these eukaryotic domains include F box and prenylation motifs, the U box domain, leucine-rich repeats, and ankyrin repeat domains (ARDs), which are protein-protein interaction domains (38–42).

The ankyrin repeat (AR) is a structural fold composed of two α -helices forming a helix-turn-helix motif. It is one of the most commonly found structural motifs in eukaryotic proteins (34, 38). Each AR-containing domain (ARD) usually contains multiple ARs (43–48), functioning predominantly as protein-protein interaction scaffolds (49, 50). Many bacterial pathogens that inject protein effectors into host cells harbor eukaryote-like ARD-containing protein effectors that interact with specific host targets (33, 51, 52). Among 58 sequenced species of *Legionella*, 1,134 ARD-containing effectors have been identified in various combinations with other eukaryotic domains (12, 14, 53).

While many *L. pneumophila* effectors are dispensable for intracellular growth of the pathogen in macrophages, we have previously shown that the AnkH ARD-containing effector is one of very few effectors required for intracellular replication in macrophages and amoebae and for intrapulmonary proliferation in the A/J mouse model (53, 54). We have also shown that AnkH is among the effector proteins that contain an asparagine

TABLE 1 Potential interacting partners identified in Y2H screen

Protein identified by yeast two-hybrid assay	Protein function
LA-related protein 7 (LARP7)	Involved in global transcription regulation
Intersectin 2 (INST2)	Adaptor protein involved in trafficking of endocytic vesicles
Ubiquitin-specific peptidase-like 1 (USPL1)	SUMO-specific isopeptidase involved in protein deSUMOylation
ANK repeat domain 18A (ANKRD18A)	Possible role in global regulation of platelet function and no.
TOX4	Involved in regulating chromatin structure and cell cycle progression
Sodium channel modifier 1 (SNCM1)	Zinc finger protein and putative splicing factor
HLA-DQA1	Involved in process of presenting antigens on cell surface

hydroxylation motif [Lxxxx(D/E)(ILVA)N(ILVA)], which is hydroxylated in human macrophages (54, 55).

While no *L. pneumophila* effectors have been shown to interfere directly with host transcription machinery, few *L. pneumophila* effectors have been identified that modulate host translation machinery. Five effectors (Lgt1, Lgt2, Lgt3, Sid1, and SidL) act on host translation machinery primarily by interfering with the eELF1A and eELF1B γ host elongation factors (56–59). In contrast, the RomA (or LegAS4) effectors are SET domain-containing proteins that directly modify host chromatin through histone modification; however, the effect on host transcription is not known (60, 61). The LegK7 effector interferes with the host Hippo signaling pathway, which results in the degradation of TAZ and YAP1 transcriptional regulators, altering the transcriptional profile of mammalian macrophages (62).

No bacterial effector has been shown to modulate the function of 7SK small nuclear ribonucleoprotein (7SK snRNP). La-related protein 7 (LARP7) is a component of the 7SK snRNP complex which controls the pausing time of polymerase (Pol) II at the initiation of transcriptional elongation at almost all metazoan genes (63–65). Binding of LARP7 to the 7SK 3'-terminal U-rich sequence protects 7SK from nucleolytic degradation (65–69). The canonical 7SK snRNP core complex consists of 7SK, LARP7, and γ -methylphosphate capping enzyme (MePCE) (63–65). Formation of the 7SK snRNP core complex enables recruitment of transcription elongation factor b (P-TEFb; Cdk9-cyclin T1 heterodimer) and HEXIM1/2 dimer to the complex (64, 67, 70–73). Binding and sequestration of P-TEFb within the 7SK snRNP complex result in inhibition of its kinase activity and continuation of the pause in Pol II transcription elongation (66, 69, 74, 75). P-TEFb is the critical factor that controls the release of paused Pol II into productive elongation at almost all metazoan genes. Various stimuli trigger the release of P-TEFb from the 7SK snRNP complex, leading to activation of its kinase activity and transition of Pol II into productive transcriptional elongation (76, 77). Our data indicate that the β -hairpin loop of the third ankyrin repeat of AnkH interacts with LARP7. The AnkH-LARP7 interaction impedes interaction of LARP7 with the 7SK snRNP complex components, which would trigger transcriptional elongation by Pol II leading to host global transcriptional reprogramming.

RESULTS

Interaction of AnkH with the LARP7 host protein. We utilized the yeast two-hybrid (Y2H) system to identify potential host cell interacting partners of AnkH. The full-length coding sequence of AnkH served as the bait construct, and the normalized universal human library was used for the prey. After mating of the two yeast strains, a total of 1,004 potentially positive clones were identified, and their growth on a selective media narrowed the number of clones representing positive results to 37. After multiple rounds of cotransformations of AnkH and the 37 positive clones, 7 potential interacting partners of AnkH were identified (Table 1). Of the seven host protein candidates, LARP7 was the only one testing positive in all cotransformations; thus, we pursued verification of its interaction with AnkH.

The LARP7 protein is a component of the 7SK snRNP complex, which enables a continued pause of Pol II elongation through sequestering and inhibiting the kinase

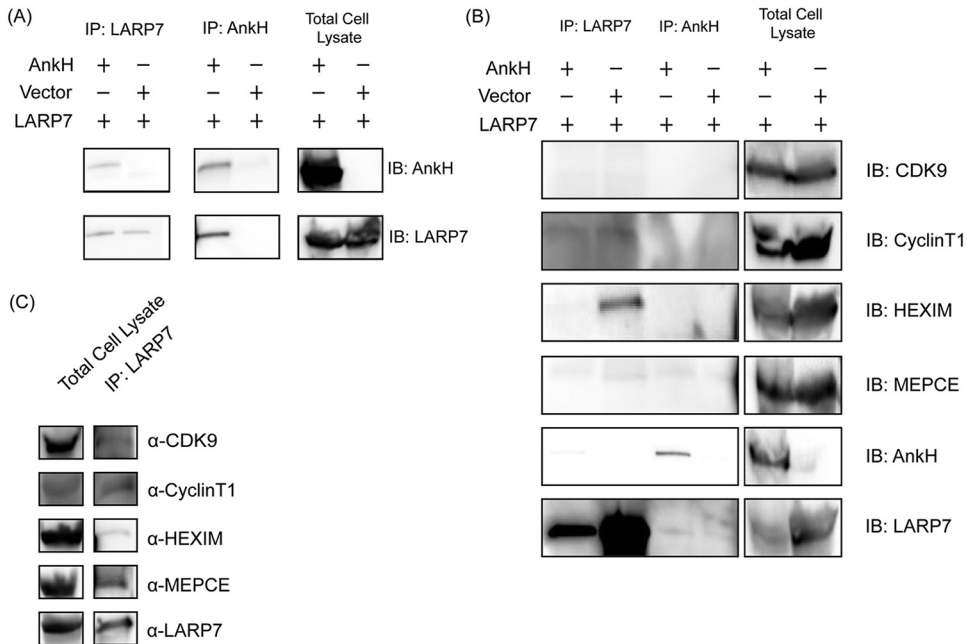


FIG 1 Interaction of LARP7 with the AnkH effector. (A) HEK293T cells were transiently transfected with 3XFLAG-AnkH or 3XFLAG-BAP and *c-myc*-LARP7 and immunoprecipitated with anti-FLAG or anti-myc antibody, and the co-IP was subjected to immunoblotting to detect the presence of AnkH and LARP7. (B) The AnkH co-IP was subjected to immunoblotting (IB) against 7SK snRNP complex components. (C) HEK293T cells were transiently transfected with *c-myc*-LARP7 and immunoprecipitated with anti-myc antibody, and the IP was subjected to immunoblotting to detect the presence of 7SK snRNP complex components. Lanes for total cell lysates of the immunoblot were imaged for less time due to a high-intensity signal. Results are representative of five independent experiments.

activity of P-TEFb (78). To confirm the AnkH-LARP7 interaction, tagged AnkH and LARP7 were cotransfected into human embryonic kidney (HEK293T) cells and subjected to reciprocal coimmunoprecipitation (co-IP) by IP of AnkH or LARP7 (Fig. 1A). The data showed that LARP7 was pulled down with AnkH, in the reciprocal co-IPs (Fig. 1A). To determine if AnkH-LARP7 interaction impacted recruitment of critical components essential for sequestration of P-TEFb in the 7SK snRNP complex, we determined whether the LARP7-AnkH complex interacted with the 7SK snRNP components. The AnkH co-IP was probed using immunoblotting for components of the 7SK snRNP complex (CDK9, cyclin T1, MePCE, HEXIM1/2). The data showed that none of the other complex components were immunoprecipitated with the LARP7-AnkH complex, similarly to the vector control (Fig. 1B). However, MePCE was immunoprecipitated with the LARP7-AnkH complex 60% of the time (3 of 5 replicates). This could have been the result of expression of MePCE and of the transient formation of the 7SK snRNP complex or could have indicated that these MePCE-positive samples were immunoprecipitated in instances where LARP7 was part of the complex and had not yet been removed from the complex via the LARP7-AnkH interaction. Importantly, in the absence of AnkH, all of the 7SK snRNP components immunoprecipitated in a complex with LARP7 (Fig. 1C). Our data show that AnkH specifically interacts *in vivo* with the LARP7 protein and that this impedes interaction of LARP7 with critical components of the 7SK snRNP complex required for the sequestration of P-TEFb in the 7SK snRNP complex.

Localization of AnkH with LARP7 to the host cell nucleus. Consistent with its role in transcription, LARP7 is localized primarily in the nucleus (78). Since AnkH interacts with LARP7, we determined whether the AnkH effector was targeted to the nucleus. HEK293T cells were transfected with a plasmid containing tagged AnkH, and subcellular localization of AnkH was examined using confocal microscopy (Fig. 2A). In 85% of transfected cells, the AnkH effector was predominantly localized to the nucleus in

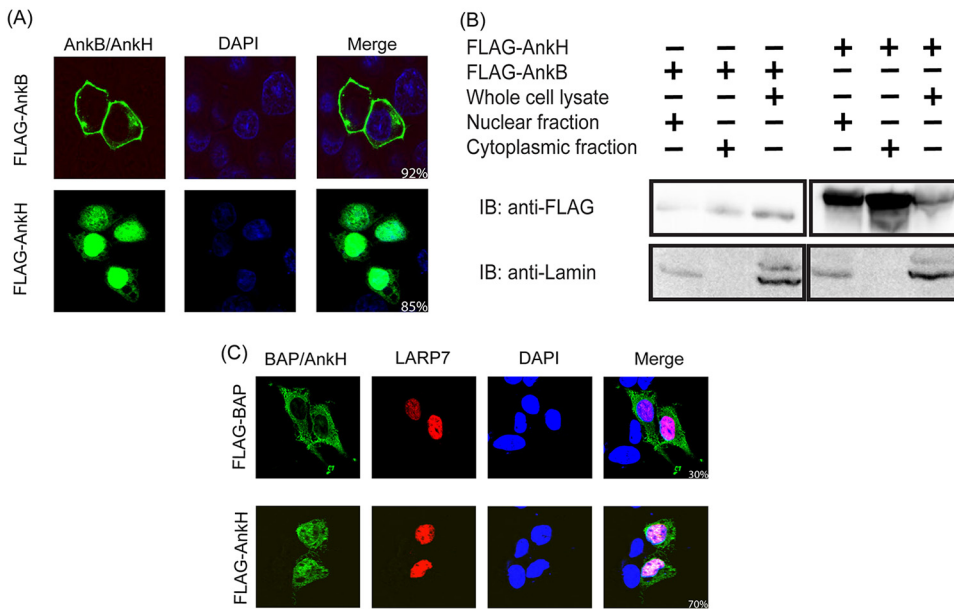


FIG 2 Localization of AnkH with LARP7 in the nucleus. (A) Representative confocal microscopy images of HEK293T cells transiently transfected with 3XFLAG-AnkH or 3XFLAG-AnkB control. The cells were labeled with anti-FLAG antibody (green), and the nucleus was stained with DAPI (blue). (B) HEK293T cells were transiently transfected with 3XFLAG-AnkH or a 3XFLAG-AnkB control and were subjected to nuclear fractionation. Cell fractions were separated by SDS-PAGE and analyzed by immunoblotting. AnkH and AnkB were detected using anti-FLAG monoclonal antibody. Fractionation was confirmed by detection of the nuclear protein lamin. (C) Representative confocal microscopy images of HEK293T cells transiently cotransfected with 3XFLAG-AnkH and *c-myc*-LARP7 or 3XFLAG-BAP and *c-myc*-LARP7. The cells were labeled with anti-FLAG (green) or anti-myc (red), and the nucleus was stained with DAPI (blue). Numbers in the merged images in panels A and C represent results of quantification of percentages of nuclear localizations of AnkH and LARP7 proteins in HEK293T cells. For panels A and C, 100 transfected cells were analyzed from multiple coverslips. Results are representative of three independent experiments performed in triplicate.

addition to showing some cytosolic localization (Fig. 2A). In contrast, the AnkB effector control was primarily (92%) localized to the plasma membrane (Fig. 2A) (40, 79).

To confirm subcellular localization of AnkH, nuclear and cytoplasmic fractions were analyzed by immunoblotting. In cells transfected with tagged AnkH, similar amounts of AnkH were present in the nuclear and cytoplasmic fractions (Fig. 2B), while the AnkB effector control was mainly localized to the cytoplasmic fraction (Fig. 2B). Cellular fractionation was confirmed using the nuclear protein lamin as a control (Fig. 2B).

To determine if AnkH and LARP7 were simultaneously localized to the nucleus, HEK293T cells were transfected with tagged AnkH and LARP7 and confocal microscopy was performed. The tagged bacterial alkaline phosphatase (BAP) was used as the control. Our data confirmed that ~70% of the cells showed simultaneous localization of AnkH and LARP7 in the nucleus (Student's *t* test; $P < 0.01$) (Fig. 2C) compared to the proportion (~30%) seen with the BAP control, which is a highly expressed protein (Fig. 2C). Our data showed that AnkH and LARP7 are localized to the nucleus, consistent with their interaction.

Role of LARP7 in intracellular replication of *L. pneumophila* in hMDMs. We have previously shown that AnkH is required for intracellular replication of *L. pneumophila* in macrophage and amoeba (53, 54). Depletion of either LARP7 or MePCE via RNA interference (RNAi) triggers 7SK degradation in cells (67, 71, 80). Since AnkH interacts with the LARP7 component of the 7SK snRNP complex, we investigated if LARP7 was also required for replication of *L. pneumophila*. We utilized a lentiviral RNAi system to knockdown expression of LARP7 in human monocyte-derived macrophages (hMDMs) that were infected with the wild-type (WT) strain of *L. pneumophila* or with the Δ *ankH* null mutant. Knockdown of LARP7 was confirmed by immunoblotting (Fig. 3A). Interestingly, when LARP7 was knocked down and cells were infected with the Δ *ankH*

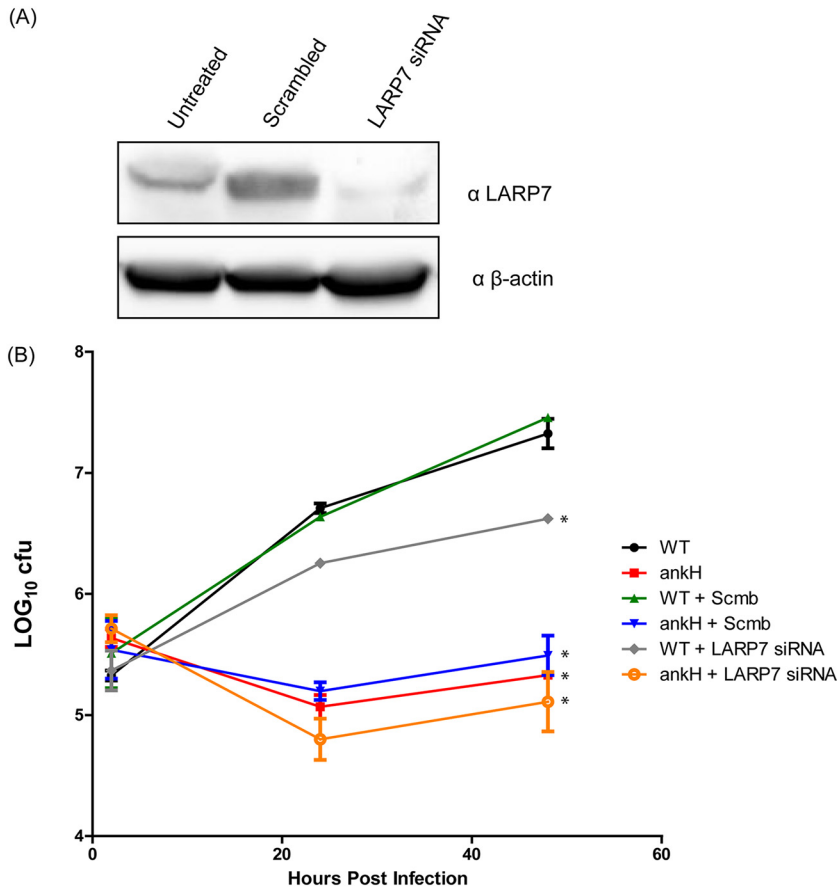


FIG 3 Requirement of LARP7 for intracellular replication of *L. pneumophila*. (A) Cells were treated with LARP7 RNAi for 24 h then infected. Knockdown of LARP7 was determined by immunoblotting with anti-LARP7 polyclonal antibody. (B) Intracellular growth kinetics of *L. pneumophila* in hMDMs treated with LARP7-specific or scrambled RNAi. The results are representative of three independent experiments performed in triplicate. Statistical analysis was performed using Student's *t* test (*, $P < 0.05$).

mutant, the defective phenotype was exacerbated. Surprisingly, the knockdown of LARP7 resulted in a partial but significant decrease in intracellular replication of the WT strain (Student's *t* test; $P < 0.05$) which was not observed in nontreated or control RNAi-treated cells (Fig. 3B). These data support our findings with respect to the role of AnkH-LARP7 interaction in intracellular replication of *L. pneumophila* in hMDMs and indicate that LARP7 is involved in transcription of genes involved in permissiveness to *L. pneumophila*.

Alteration of host global transcription by AnkH. Our data showed that the LARP7-AnkH complex impedes interactions of LARP7 with critical components of the 7SK snRNP complex required for the sequestration of P-TEFb in the 7SK snRNP complex, which indicates the presence of an active P-TEFb kinase and release of Pol II from pause sites, and transitions into productive transcriptional elongation (67, 78). We utilized transcriptome sequencing (RNA-Seq) to examine modulation of global gene expression in hMDMs infected with either the WT strain or the Δ ankH null mutant. The data showed that AnkH had a dramatic effect on global transcription of *L. pneumophila*-infected hMDMs, with a total of 405 genes that were differentially regulated in cells infected with the WT strain compared to the Δ ankH mutant; the top 10 of each (based on log fold change) are listed in Table 2 (a full list is provided in Table S3 in the supplemental material [see also Table S4]). MetaCore was used to determine which pathways were differentially regulated based on *P* values. Certain cellular pathways, including the apoptosis pathway and the autophagy pathway, and certain signaling pathways, including the STK3/4 pathway and Jun N-terminal protein kinase (JNK)

TABLE 2 Top 10 upregulated genes and top 10 downregulated genes in cells infected with *ankH* mutant compared to cells infected with WT

Gene symbol (description)	Log ₂ FC ^a
HSPA1B (heat shock 70-kDa protein 1B)	+2.9979
EGR1 (early growth response 1)	+2.25815
DNAJB1 (DnaJ [Hsp40] homolog, subunit B, member 1)	+1.51215
DUSP1 (dual-specificity phosphatase 1)	+1.24951
FOS (FBJ [Finkel-Biskis-Jinkins] murine osteosarcoma viral oncogene homolog)	+1.15258
TDO2 (tryptophan metabolism)	+1.01074
MS4A4E (membrane-spanning 4-domains, subfamily A, member 4E)	+2.36464
PKIB (protein kinase inhibitor beta)	+1.33129
PEG3 (paternally expressed 3)	+2.64637
GRIK2 (glutamate receptor, ionotropic, kainate 2)	+1.78851
TMC8 (transmembrane channel-like 8)	-2.75204
HMHA1 (histocompatibility [minor] HA-1)	-1.99385
DAPK3 (death-associated protein kinase 3)	-1.91505
PDLIM2 (PDZ and LIM domain 2)	-1.79007
SDF2L1 (stromal cell-derived factor 2-like 1)	-1.65596
TOR2A (torsin family 2, member A)	-1.62058
LMF2 (lipase maturation factor 2)	-1.59493
NOTCH3 (Notch 3)	-1.57732
IL-27 (interleukin 27)	-1.55472
CPSF1 (cleavage and polyadenylation-specific factor 1)	-1.89935
TMC8 (transmembrane channel-like 8)	-2.75204

^aLog₂ FC, log₂ fold change.

pathway, were downregulated in an AnkH-dependent manner, indicating negative regulation of these pathways by AnkH during infection (Table 3). Transcription and immune response pathways were downregulated in cells infected with the Δ *ankH* null mutant compared to cells infected with the WT strain, indicating their upregulation by AnkH (Table 3). These data show that AnkH triggers a dramatic reprogramming of cellular transcription and that the reprogramming is most likely mediated by interaction with several host substrates, one of which is LARP7.

The crystal structure of AnkH. AnkH is one of a few of the ~330 *Legionella* effectors required for intracellular growth within amoebal hosts and human macrophages (9, 32). To gain greater insight into possible cellular functions of AnkH, we determined its three-dimensional crystal structure. AnkH is an α/β -fold protein and contains a total of 21 α -helices and seven β -strands (Fig. 4A). AnkH consists of 3 domains: N-terminal ankyrin domain (α 1 to α 8; see red data in Fig. 4A), the middle domain (α 10 to α 17 and β 3 to β 7; cyan and magenta), and the cap domain (β 1 to β 2, α 9, and α 18 to α 21; wheat (53, 54)). The N-terminal domain contains ankyrin repeats with four helix-turn-helix repeats (α 1 to α 8, residues 1 to 122) (Fig. 4B). The first repeat is somewhat distorted and has shorter α -helices. The ARD is followed by a 4-turn-long helix α 9 and an extended β -hairpin (β 1 to β 2, residues 123 to 162) leading to the middle domain (Fig. 4A). This domain (residues 163 to 361) contains a central 5-stranded antiparallel β -sheet, β 3 to β 7, and is extended by the presence of helix α 12.

TABLE 3 Upregulated and downregulated pathways in cells infected with *ankH*^a

Upregulated pathway	P value	Downregulated pathway	P value
Development-positive regulation of STK3/4 (Hippo) pathway and negative regulation of YAP/TAZ function	1.338e-9	Transcription, HIF-1 targets	2.822e-15
Transport clathrin-coated vesicle cycle	2.291e-9	Immune response, IL-3 signaling via JAK/STAT, p38, JNK, and NF κ B	1.745e-14
Apoptosis and survival, FAS signaling cascades	9.334e-9	Immune response, IL-1 signaling pathway	1.270e-11
Immune response, antigen presentation by MHC class I (cross-presentation)	5.959e-8	Immune response, IL-10 signaling pathway	1.397e-11
Signal transduction, JNK pathway	6.740e-8	Apoptosis and survival, anti-apoptotic TNF/NF κ B/Bcl-2 pathway	2.725e-11

^aFAS, fatty acid synthase; JNK, Jun N-terminal protein kinase; IL-3, interleukin-3; MHC, major histocompatibility complex; TNF, tumor necrosis factor.

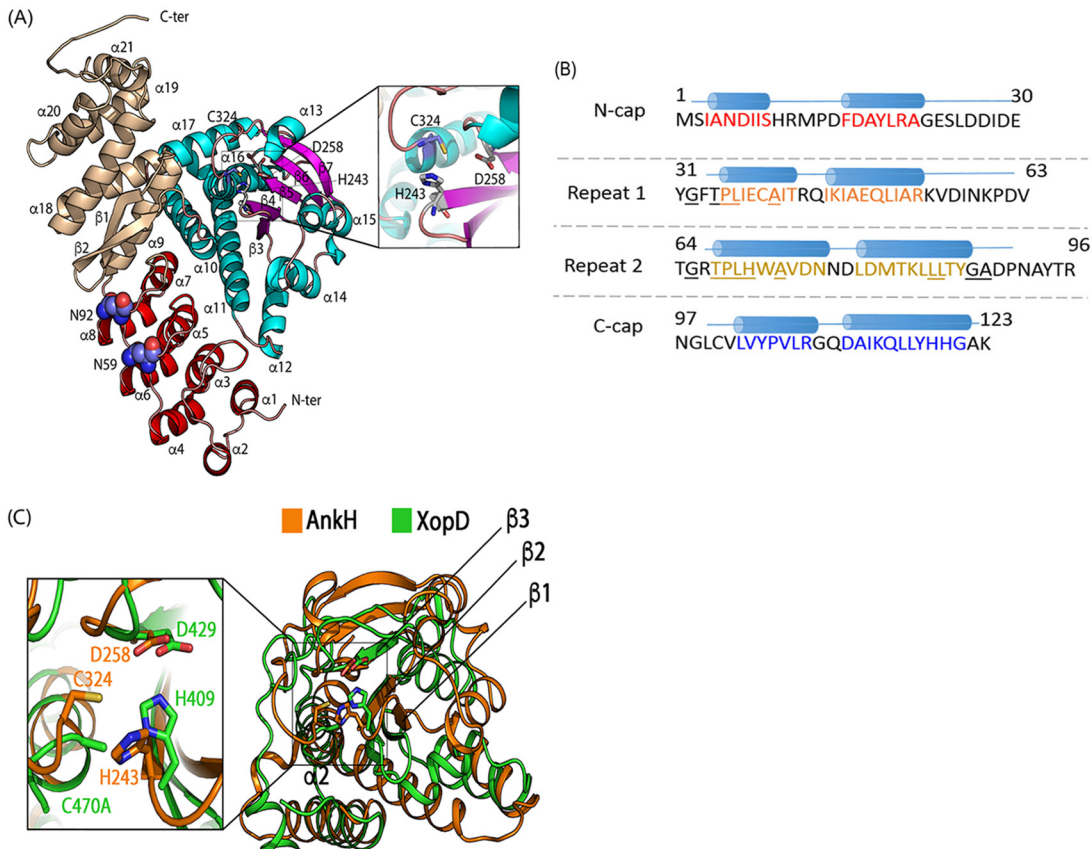


FIG 4 The crystal structure of AnkH. (A) AnkH consists of 3 domains: N-terminal ankyrin domain ($\alpha 1$ to $\alpha 8$; red), the cysteine proteinase-like domain ($\alpha 10$ to $\alpha 17$ and $\beta 3$ to $\beta 7$; cyan and magenta), and the cap domain ($\beta 1$ and $\beta 2$, $\alpha 9$, and $\alpha 18$ to $\alpha 21$; wheat). The inset shows a closeup of putative catalytic triad residues H243, D258, and C324. The HIF hydroxylation sites (N59 and N92) are located within the N-terminal domain and are shown in a sphere representation (blue and red). (B) Primary sequence of ankyrin domain. The length of each ankyrin repeat was determined using the consensus sequence based on statistical analysis of 4,000 ankyrin repeat sequences from the PFAM database as proposed by Mosavi et al. (47). Highlighted (colored) letters correspond to α -helices for each domain. The conserved residues are underlined, and the α -helices are shown as cylinders. (C) Superposition of AnkH with *Xanthomonas* XopD C470A mutant. The cartoon diagram represents superposition of the AnkH cysteine protease-like domain (residues 163 to 342; orange) and the *Xanthomonas* XopD C470A mutant (PDB identifier ID 2OIX, residues 336 to 515; green). The three β -strands and two α -helices that form the core of the domains and overlap well are marked. The inset shows a closeup of the catalytic triad. In AnkH, these residues are His243, Asp258, and Cys324; in XopD, these residues are His409, Asp429, and Cys470.

The β -sheet is flanked by two layers of two helices (inner, $\alpha 11$ and $\alpha 16$; outer, $\alpha 10$ and $\alpha 17$) on one side and two helices ($\alpha 14$ and $\alpha 15$) on the other side. The C-terminal domain (residues 362 to 461) contains a five-helix bundle (Fig. 4A) and packs tightly together with $\alpha 9$ and the following β -hairpin, forming one domain. The N-terminal and C-terminal domains pack end to end into a crescent shape (Fig. 4A). The middle domain forms an independent insertion attached to the side of the ARD that typically functions as the protein binding surface. The long loops emanating from the ARD, usually involved in protein-protein interactions, face the middle domain.

The inserted middle domain of AnkH has a cysteine protease fold. To gain insight into possible functions of the middle and cap domains, we searched for their structural homologs using the Dali server (81). The middle (insertion) domain showed structural similarity to several proteins with a cysteine protease fold, albeit with relatively low scores. This cysteine protease-like domain (CPLD) is most similar to the outer protein D (XopD; PDB identifier [ID] 2OIX) from bacterial plant pathogen *Xanthomonas campestris* pv. *vesicatoria* (82–84) (Fig. 4C). It also shows similarity to a domain of another *Legionella pneumophila* effector, RavZ (85, 86).

XopD belongs to the ubiquitin-like-specific protease 1 family (87) and is classified within clan CE in the MEROPS database (88), with the catalytic triad arranged in the

TABLE 4 Point mutations generated in different domains of AnkH^a

ANK1 mutation(s)	ANK2 mutation(s)	ANK3 mutation(s)	Asn hydroxide mutation(s)	Cysteine-protease mutation(s)
E30T	V63Y	R96A	N59A	H243D
Y31S	T64E	N97V	N92A	D258A
F33A				C324S

^aANK1, ANK2, and ANK3 designate ankyrin repeat 1, ankyrin repeat 2, and ankyrin repeat 3.

following order: histidine, glutamate/aspartate/asparagine, and cysteine. Cysteine functions as a nucleophile, while histidine serves as a general base and is in turn stabilized by glutamic acid/aspartic acid (87). The structure-based sequence identity between the aligned regions of CPLD and XopD is only ~12%; nevertheless, three β -strands and two α -helices are structurally similar between AnkH and XopD (Fig. 4C), with His243, Asp258, and Cys324 of AnkH superposed on the catalytic triad of XopD. The histidine resides on the N-terminal end of the conserved strand within the protease fold (β 4 in AnkH; Fig. 4A). The stabilizing aspartic acid sits at the C-terminal end of the conserved antiparallel strand (β 5 in AnkH; Fig. 4A). The cysteine nucleophile is at the end of a long loop leading to the penultimate helix of the protease fold (Fig. 4A). The orientation of these three side chains in AnkH deviates from the active configuration, and a small rearrangement of the triad side chains has to occur to attain the active state (Fig. 4C). The fold of AnkH CPLD was recognized due to very low sequence identity to other cysteine protease and is not yet classified in the peptidase database MEROPS (89), which already includes several other peptidases from the *Legionella* species (data not shown).

Structure-function analysis of AnkH. The structure of AnkH suggested that it binds a cellular target(s) through the β -hairpin loops within ARD and has a predicted proteolytic activity (Fig. 4A). To better understand the roles of the AnkH domains and to validate its structure, a total of 12 residues were chosen for single substitutions based on their location within a specific domain (Table 4; see also Fig. 4). The substituted residues included residues on the extended β -hairpin loops of ARs (Fig. 1; see also Fig. 4B), the putative cysteine protease catalytic triad and two asparagine residues (N59 and N92) that have been reported to undergo asparagine hydroxylation, which impacts protein-protein interactions (55). Each of the ARDs is illustrated in Fig. 5A. Panels B and C of Fig. 5 illustrate the location of each substitution made within the ARDs. The mutations had no detectable effect on stability of the variant proteins in *L. pneumophila* (Fig. 5D) or during transient transfection (Fig. 5E).

HEK293T cells were cotransfected with LARP7 and either native AnkH or AnkH containing substitutions within the β -hairpin loops of the ARDs and were then subjected to immunoprecipitation. Our data showed that substitutions of residues within the ARD3 (specifically, Asn97) diminished the LARP7-AnkH interaction (Fig. 5F). In contrast, substitution of residue 30, 31, 33, 63, 64, or 96 resulted in enhanced binding between LARP7 and AnkH (Fig. 5F).

In order to determine if the substitutions affected the function of AnkH in intracellular replication of *L. pneumophila*, hMDMs were infected with the WT strain, the $\Delta ankH$ null mutant, the $\Delta ankH$ mutant complemented with the WT allele of *ankh*, or the substitution variants of AnkH. Our data showed that substitution in the β -hairpin loop of ARD3, which led to reduced binding of LARP7 to AnkH, resulted in reduced intracellular growth of *L. pneumophila* (Fig. 6). All other residues selected for substitutions were partially required for AnkH function in intracellular replication, since introducing these mutations resulted in various degrees of partial replication defect compared to the WT strain (Student's *t* test; $P < 0.05$) (Fig. 6) (Table 4). Therefore, we conclude that the ARD (in particular, Asn97), the cysteine-like protease domain, and the asparagine hydroxylation motifs are all required for the function of AnkH in intracellular proliferation of *L. pneumophila* within hMDMs.

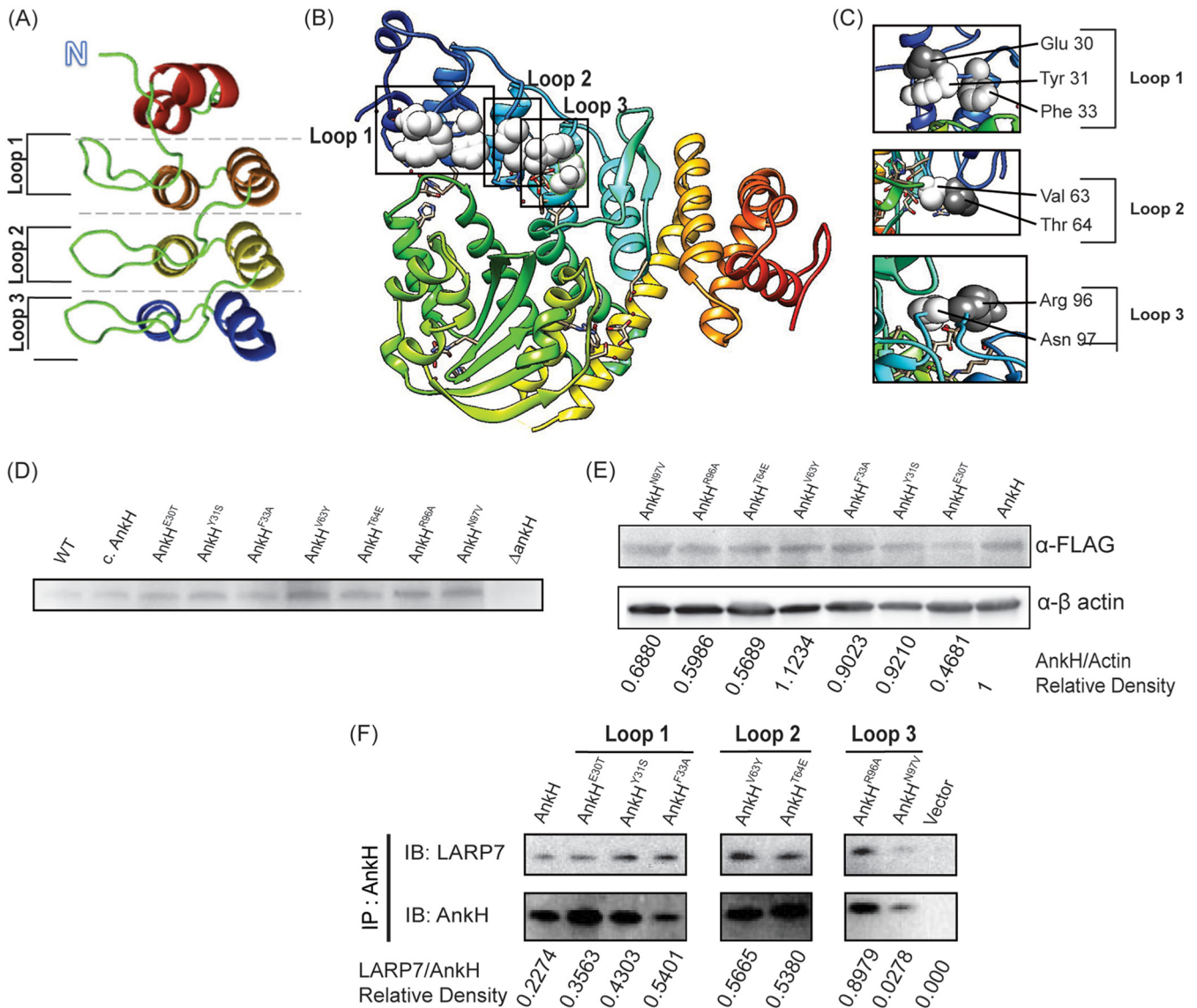


FIG 5 Substitutions in ARDs alter binding efficiency of AnkH and LARP7. (A) The ankyrin domain of AnkH shown as a ribbon diagram. The ankyrin domain consists of four ankyrin repeats: N-cap, repeat 1, repeat2, and C-cap. (B and C) Crystal structure of AnkH illustrating the whole structure (B) and insets representing different locations within the ARDs where residues were substituted (C). (D) Bacterial lysates from WT *L. pneumophila* and each of the AnkH substitution mutant strains were tested by immunoblotting for AnkH to determine protein stability. Cell lysates were subjected to immunoblotting to detect the presence of AnkH using goat anti-AnkH (53, 56). Equal numbers of bacteria were lysed for each strain. (E) HEK293T cells were transiently transfected with 3XFLAG-AnkH or the indicated 3XFLAG-AnkH substitution mutants and *c-myc*-LARP7. Densitometry was determined in accordance as actin ratio. (F) Cell lysates were immunoprecipitated with anti-FLAG antibody, and the co-IP was subjected to immunoblotting to detect the presence of AnkH and LARP7. Densitometry of the blots was determined as the LARP7-to-AnkH ratio.

DISCUSSION

Among the ~18,000 effectors of *Legionella* genus, AnkH is the only one conserved among all *Legionella* species as well as other pathogens that harbor the Dot/Icm secretion system (12, 14). While many *L. pneumophila* effectors are dispensable for intracellular growth of the pathogen in macrophages (24, 29, 32, 90), the AnkH effector plays a role in intracellular growth of *L. pneumophila* within amoeba hosts and within macrophages (53, 54). In addition, the high level of conservation of AnkH among many pathogenic obligate and facultative intracellular species of bacteria (12, 14) suggests its role in modulating an evolutionarily conserved eukaryotic process exploited by the various obligate and facultative intracellular pathogens that translocate the AnkH effector by the Dot/Icm T4SS. The results of a BLAST search (91) performed with the

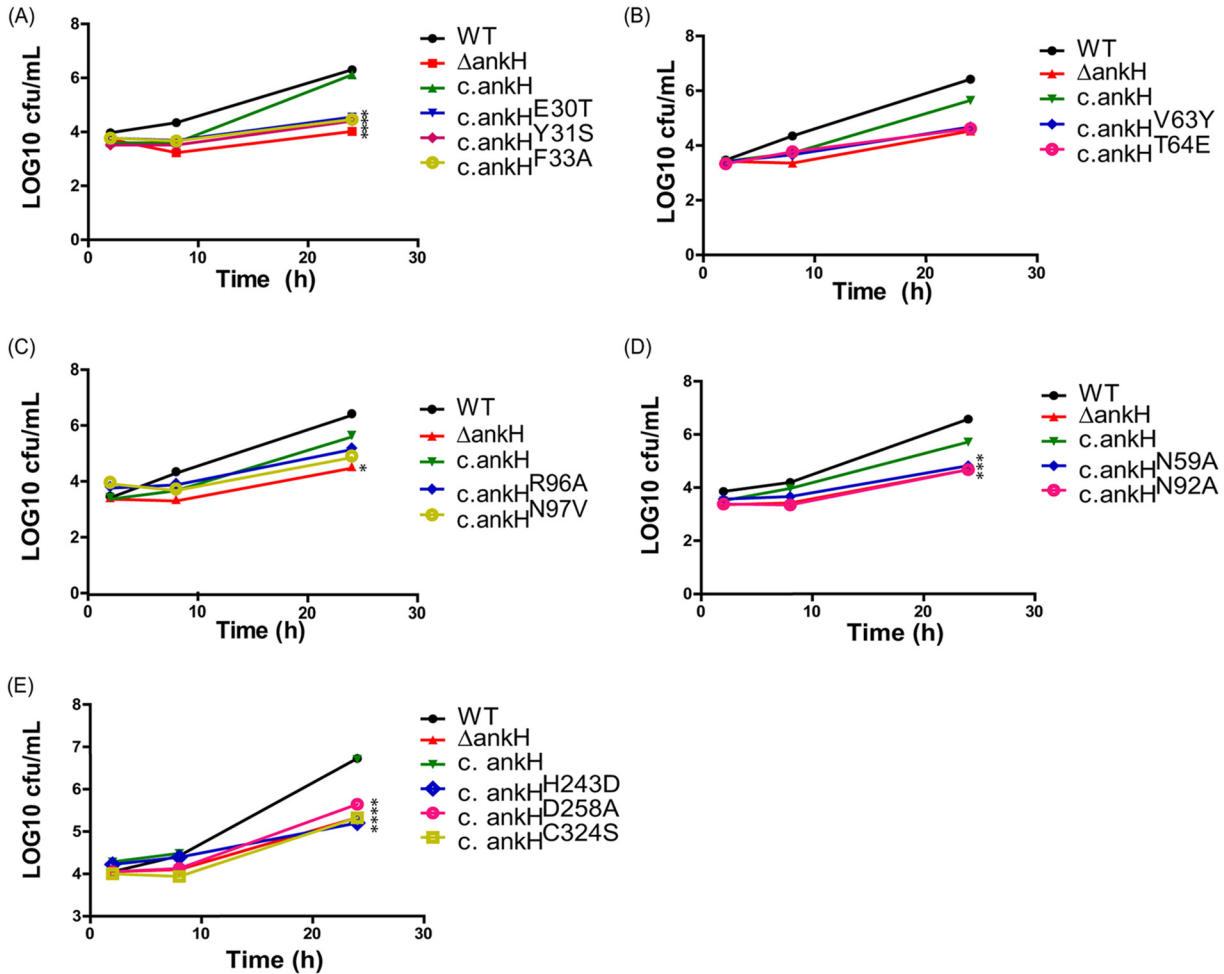


FIG 6 Structure-function analysis of AnkH in intracellular growth of *L. pneumophila* within hMDMs. Intracellular growth kinetics were determined for the WT strain, the *ankH* mutant, or the *ankH* mutant complemented with the WT allele (c.*ankH*) or with single and multiple substitution variants as indicated. All strains represented in all the panels were tested using the same WT control. (A) Mutations within first ANK repeat. (B) Mutations within second ANK repeat. (C) Mutations within third ANK repeat. (D) Mutations within the asparagine hydroxylation motif. (E) Mutations within the cystine-like protease pocket. The results are representative of three independent experiments performed in triplicate. Statistical analysis was performed using Student's *t* test (*, $P < 0.05$).

AnkH sequence show that, in addition to various *Legionella* species, homologous proteins are also found in *Gammaproteobacteria* species, *Coxiella* species, *Candidatus berkiella*, *Rickettsia* species, *Aquicella*, and *Tatlockia micdadei*. In most cases, the homologs contain all domains; in some cases, the C-terminal domain is partially or fully missing. All these homologs conserve the His-Asp-Cys catalytic triad residues, which are embedded in conserved patterns as follows: r**GH**a, **D/NR**g and **GNCSWANV** (which are preserved down to the ~30% levels of sequence identity with AnkH CPLD domain) (boldface highlighting represents the catalytic triad).

Since ARDs can potentially bind to multiple protein partners, it is likely that AnkH interacts with several other host proteins in addition to LARP7. Through the yeast two-hybrid screening, we identified six other host proteins with which AnkH might interact. Using co-IP, we confirmed that the host LARP7 component is an interaction partner for AnkH in HEK293T cells. Since residues within the β -hairpin loops of the ARDs are involved in binding to substrates, our data are consistent with these findings, as we have shown that substitution in β -hairpin loops of the ARD3 results in reduced binding of AnkH to LARP7, indicating that this loop is the more likely one to bind the LARP7 component of the 7SK snRNP complex, which controls pausing of Pol II at the initiation of transcriptional elongation (see model in Fig. 7) (63–65). Formation of the 7SK snRNP

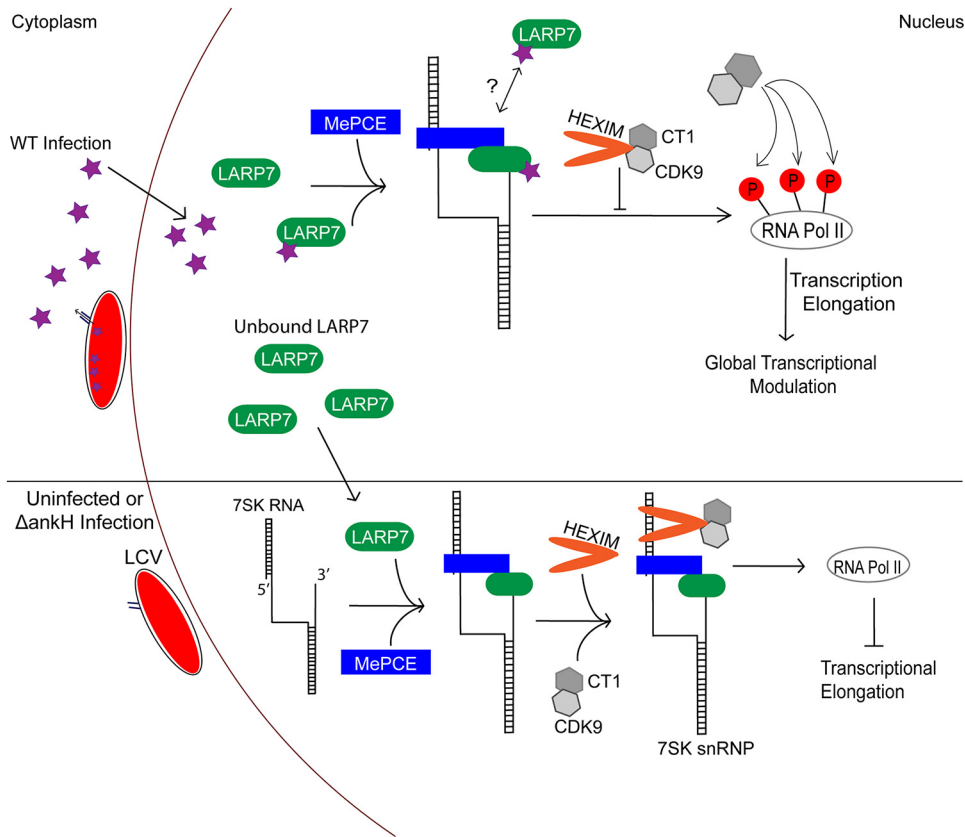


FIG 7 Working model of Ankh-LARP7 interaction. In uninfected cells or during $\Delta ankH$ mutant infection of HEK293T cells, formation of the 7SK snRNP begins when the 5' methyl capping enzyme (MePCE) and LARP7 are recruited to the 7SK snRNA, forming the core of the 7SK snRNP. After core formation, the HEXIM1/2 dimers as well as the P-TEFb (Cdk9 and cyclin T1) kinase are recruited to complete the 7SK snRNP complex, which prevents transcription elongation by holding RNA polymerase (Pol) II in a paused state. During infection with WT *L. pneumophila*, Ankh is trafficked to the nucleus, where it interacts with a portion of available LARP7 in the cell. The interaction between Ankh and LARP7 results in a partial inhibition of the 7SK snRNP complex function, leading to enhanced transcriptional elongation by blocking the recruitment of HEXIM1/2 and P-TEFb. The remaining LARP7 present in the cell (the fraction that does not interact with Ankh) is available to interact with other components of the 7SK snRNP complex to pause transcription elongation by preventing P-TEFb from phosphorylating RNA polymerase 2, keeping the polymerase in a paused state. This balance between the pause and relief of the pause in transcriptional elongation results in transcriptional reprogramming within host cell that enhance permissiveness to *L. pneumophila* infection. There are likely other unidentified substrates of Ankh that could aid in this process or the could act independently of the interaction with LARP7. The effect on amoeba host transcription by Ankh may be different from that seen with human macrophages.

core complex (7SK, LARP7, and MePCE) enables recruitment of P-TEFb and HEXIM1/2 to the complex (64, 67, 70–73). Binding and sequestration of P-TEFb within the 7SK snRNP complex result in inhibition of its kinase activity and continuation of the pause in Pol II transcription elongation (66, 69, 74, 75). Various stimuli trigger the release of P-TEFb from the 7SK snRNP complex, leading to activation of its kinase activity and transition of Pol II into productive transcriptional elongation (76, 77). Our data indicate that LARP7 interacts with the β -hairpin loop of the third AR of Ankh, which impedes 7SKsnRNP complex formation, leading to productive transcriptional elongation by Pol II and host global transcriptional reprogramming. Our data show that there is an upregulation in pathways regulating transcription and immune responses in the presence of Ankh. In the absence of Ankh, however, there is an upregulation in pathways involved in vesicular trafficking, autophagy, and apoptosis. These observations support our findings with respect to the role of Ankh-LARP7 interaction in modulating the function of the 7SK snRNP complex in human macrophages, but the effect of Ankh on host global transcription is likely impacted by interaction of Ankh with other host targets. The range of pathogenic effectors that modulate host transcription machinery is limited,

and the manipulation of the host 7SK snRNP complex via LARP7-AnkH interaction identifies a novel effector mechanism for host transcription control during infection. However, it is not known whether interaction of AnkH-LARP7 and potentially other host targets evolved during interaction of *L. pneumophila* with various protist hosts in the aquatic environment to modulate amoeba host-specific gene transcriptions that are highly conserved through evolution (12, 14, 32). It is highly possible that some of the transcriptional activity impacted by interaction of AnkH with LARP7 and other host targets in human macrophages may simply represent an evolutionary accident (12, 14, 32). Since knockdown of LARP7 resulted in a significant decrease in the intracellular replication of both the WT strain and the $\Delta ankH$ null mutant of *L. pneumophila*, it is likely that the AnkH-LARP7 interaction promotes transcription of genes involved in permissiveness to *L. pneumophila* in evolutionarily distant hosts. It was unexpected that LARP7 knockdown caused a significant decrease in intracellular replication of $\Delta ankH$ mutant. This could be explained by the hypothesis that AnkH does not interact with all LARP7 components available within a host cell, which could create a balance between the pausing of transcription elongation and relief of the pause in elongation that creates a favorable environment for *L. pneumophila* replication. When AnkH is deleted and LARP7 is knocked down, there is no longer a transcriptional balance, which results in the decrease in replication, likely as the result of alteration of many processes involved in permissiveness of the host cell to *L. pneumophila*.

The crystal structure revealed that AnkH contains four ARs and has two asparagine hydroxylation motifs located on the outer surface of the ARD in addition to the cysteine like protease pocket. Our data show that the predicted protease catalytic triad is essential for the function of AnkH, but we were not able to detect protease activity *in vitro* for AnkH purified from *Escherichia coli*. We speculate that the lack of detectable protease activity *in vitro* was likely due to the closed nature of the catalytic pocket of purified AnkH, suggesting a requirement of its binding to a substrate *in vivo* to open the pocket for catalysis. The ARDs are involved in protein-protein interactions by acting as a scaffold for protein binding. ARD-containing proteins can typically bind to one or more targets (38, 46). The ARDs containing multiple ankyrin repeats form crescent-like structures and contact their binding partners on the concave side that is formed from the inner short helices and the long β -hairpin/loop regions connecting the ankyrin repeats (92). Several residues on the putative target binding side of AnkH ARD that are located on the tips of the interrepeat loops are required for the function of AnkH in intracellular replication of *L. pneumophila*. These side chains are exposed to the solvent and aside from Tyr31 and Asn97 and are not in contact with the cysteine protease-like domain. Therefore, mutation of these residues likely disrupts the ability of AnkH to interact with LARP7 or other specific host targets. The mutation of Asn97 in particular led to a decrease in the ability of AnkH to bind LARP7, while mutations of other residues led to an enhanced binding, indicating that Asn97 is important for the AnkH-LARP7 interaction.

We have previously shown that AnkH is hydroxylated at N59 (55). We have also shown that the host FIH (factor inhibiting HIF [hypoxia-inducible factor]) asparagine hydroxylase localizes to the LCV and is involved in hydroxylating another *L. pneumophila* effector, AnkB (55). Asparagine hydroxylation of AnkB is also required for the function of the AnkB effector in intracellular replication of *L. pneumophila* (55). The asparagine hydroxylation motif is commonly found in ARDs and serves as a target sequence(s) for the FIH asparagine hydroxylase (93, 94), which is responsible for hydroxylating an asparagine residue within this motif (55). This hydroxylation can act as a molecular switch for protein-protein interactions by either inhibiting or strengthening the interaction (94–96). The N59 and N92 residues of ankH are located at the beginning of the loop connecting two neighboring ARDs. Our data show that the asparagine hydroxylation motifs are important for the function of AnkH in the intracellular replication. A possible explanation for the role of this modification is represented by the structure of the ankyrin domain of the mouse notch 1 with this modification (PDB ID: 2QC9) (97). The HIF-hydroxylated asparagine is located at a sharp

bend of the backbone, and hydrogen bonds through the added hydroxyl with the aspartic acid side chain two residues back and located at the other corner of the bend. It has been suggested that this additional hydrogen bond might help to stabilize the loop in the ARD (97). Equivalent aspartic acids are found in AnkH at positions 57 and 90, two back from the asparagines. Therefore, a similar possibility of stabilization of the inter-ARD loops has to be considered for AnkH as a means to strengthen the interaction with its cellular target.

In summary, AnkH is targeted to the nucleus, where it interacts with LARP7 and likely other host targets, leading to reprogramming of host transcription to promote intracellular bacterial growth. This is mediated, at least in part, by the effect of AnkH-LARP7 interaction and abolishment of interaction of LARP7 with critical subunits of the 7SK snRNP complex essential for its negative transcriptional elongation, leading to host global transcriptional reprogramming. The conservation of AnkH in intracellular pathogens harboring the Dot/Icm T4SS and its involvement in a conserved pathway support the idea of the AnkH-LARP7 interaction and its partial effect on reprogramming global host transcription, which is likely impacted by interaction of AnkH with other host targets. It is most likely the AnkH-dependent host transcriptional reprogramming that explains the unique consequences in various protist hosts compared to human macrophages. The crystal structure of AnkH shows that it contains an ARD with four ankyrin repeats containing two asparagine hydroxylation motifs, a cysteine protease-like domain, and a C-terminal domain of unknown function. Critical residues in the ARD and the cysteine protease-like domains identified from the structure are shown to be required for AnkH-LARP7 interaction and to function of AnkH in intracellular replication.

MATERIALS AND METHODS

Bacterial strains and cell culture. *L. pneumophila* strain AA100/130b (BAA-74; American Type Culture Collection) and the isogenic *dotA* and *ankH* mutants and complemented *ankH* mutants were grown on buffered charcoal yeast extract (BCYE) agar plates for 3 days at 37°C prior to use in infections, as described previously (38). *E. coli* strain DH5 α was used for cloning purposes. Human monocyte-derived macrophages (hMDMs) were cultured using RPMI 1640 media (Gibco), as described previously (41). Maintenance of HEK293T cells was performed as previously described (41). All methods were carried out and approved in accordance to the University of Louisville Institutional Review Board guidelines, and blood donors gave informed consent as approved by the University of Louisville Institutional Review Board (IRB no. 04.0358).

DNA manipulations. DNA manipulations and restriction enzyme digestions were performed using standard procedures (41, 98). Restriction enzymes and T4 DNA ligase were purchased from NEB (Madison, WI). Plasmid preparations were performed with a PureLink HiPure Plasmid Maxiprep kit (Invitrogen). Purification of DNA fragments from agarose gels for subcloning was carried out with a QIAquick gel purification kit (Qiagen Inc., Valencia, CA). Generation of AnkH substitution mutants was achieved using primers listed in Table S1 and described previously (41, 54).

Transfection of HEK293T cell. HEK293T cells were grown to ~70% confluence and plated onto poly-L-lysine-treated 24-well plates. Following 24 h of incubation, HEK293T cell monolayers were transfected with ~2 μ g of plasmid DNA/well by using polyethylenimine (Polysciences) and Opti-MEM (Gibco) for 24 h, as described previously (33, 54). The *c-myc*-LARP7 plasmid was a gift from B. Matija Peterlin, University of California, San Francisco.

Confocal laser scanning microscopy. Processing of transfected cells for confocal microscopy was performed as we described previously. Briefly, monolayers were permeabilized and fixed using 100% methanol held at -20°C for 5 min and were then blocked and labeled with mouse-anti-FLAG (Sigma) (1/200 dilution in 3% bovine serum albumin [BSA]-phosphate-buffered saline [PBS]) and rabbit-anti-Myc (Proteintech) (1/200 dilution in 3% BSA-PBS). Cells were counterlabeled with Alexa Fluor 488 anti-mouse antibody (Invitrogen) (1/4,000 dilution in 3% BSA-PBS), Alexa-Fluor 555 anti-rabbit antibody (Invitrogen) (1/4,000 dilution), and DAPI (4',6-diamidino-2-phenylindole) to stain the nuclei. Monolayers were examined by confocal microscopy. A total of 100 cells for each replicate were counted to determine the presence or absence of localization.

Intracellular replication. The wild-type strain, the *dotA* and *ankH* isogenic mutants, and the complemented *ankH* mutants were grown on BCYE agar for 3 days at 37°C prior to infection and used to infect hMDMs. A total of 1×10^5 host cells (hMDMs) per well were plated in 96-well plates and infected with *L. pneumophila* at a multiplicity of infection (MOI) of 10 for 1 h and then treated for 1 h with gentamicin to kill remaining extracellular bacteria. Over a 24-h time course, the host cells were lysed with sterile water and *L. pneumophila* CFU counts were determined by plating serial dilutions onto BCYE agar. Experiments were performed in triplicate.

Yeast two-hybrid (Y2H) analysis. A Matchmaker gold two-hybrid system (Clontech) was used to screen host proteins that interact with the AnkH protein per the instructions of the manufacturer. Full-length AnkH coding sequence was amplified, subjected to sequencing, cloned into the pGBKT7 bait

vector (Clontech), and transformed into yeast strain AH109 (Clontech). A normalized universal human cDNA library in pGADT7 was purchased (Clontech) for use as potential prey targets. The library and bait containing AH109 were mated, and the resulting colonies were screened per the instructions of the manufacturer. Plasmids from positive clones were isolated using yeast lysis buffer and glass beads. Isolated prey plasmid and bait plasmid were used to cotransform the AH109 yeast strain. Transformants were selected by growing the yeast on SD medium lacking His, Leu, and Trp (SD-His/-Leu/-Trp) (Clontech). Colonies that tested positive were then transferred to SD-Ade/-His/-Leu/-Trp plates containing 5-bromo-4-chloro-3-indoxyl- α -D-galactopyranoside (X- α -Gal) (GoldBio). Blue colonies were selected for plasmid isolation. Isolated plasmids were then sequenced to identify the human genes.

In vivo coimmunoprecipitation. HEK293T cells were transfected with 3XFLAG-AnkH, BAP, and *c-myc*-LARP7 for 24 h and collected in lysis buffer, as described previously (79, 99). FLAG-tagged and myc-tagged proteins were immunoprecipitated by using anti-FLAG M2 magnetic beads (Sigma) or SureBeads protein G magnetic beads (Bio-Rad) cross-linked with anti-myc antibody (Proteintech).

Antibodies and Western blot analysis. Immunoprecipitated proteins were heated at 99°C for 5 min in sample buffer, separated by the use of 10.4% to 15% SDS-PAGE (Bio-Rad), and transferred onto a polyvinylidene difluoride (PVDF) (Bio-Rad) membrane, as described previously (99). Anti-Flag (Sigma) used at 1:1,000 dilution and anti-myc (60003-2-Ig) (Proteintech) used at 1:1,000 were incubated overnight in 8% milk at 4°C. Anti-LaminB (13435) (Cell Signaling) was used at a 1:1,000 dilution. Anti-HEXIM1 (15676-1-AP), anti-LARP7 (17067-1-AP), and anti-MePCE (14917-1-AP) were purchased from Proteintech and used at a 1:500 dilution. Anti-CDK9 (sc-13130) was purchased from Santa Cruz and used at a dilution of 1:200. Anti-cyclin T1 (sc-271348) was purchased from Santa Cruz and used at a dilution of 1:100. Goat anti-AnkH antiserum was produced at Cocalico Biologics and was used at a dilution of 1:100 (53, 54).

RNA isolation, reverse transcription, and real-time PCR. Total RNA was extracted using TRIzol reagent (Invitrogen). cDNA synthesis was performed with 1 μ g of total RNA using an iScript cDNA synthesis kit (Bio-Rad) according to the manufacturer's instructions. Endogenous mRNA levels were measured by real-time PCR analysis based on SYBR green detection (Fermentas) with a Bio-Rad MiniOpticon real-time PCR system.

RNA-Seq. Libraries were prepared using a TruSeq stranded mRNA LT sample prep kit (set A or set B) with poly(A) enrichment (Illumina). One microgram of sample (in a volume of 50 μ l) were treated with RNA purification beads and denatured for 5 min at 65°C. The supernatant was then discarded, and the beads were washed with bead wash buffer. Captured polyadenylated RNA was eluted using elution buffer at 80°C for 2 min. mRNA was further purified in a second bead cleanup and was fragmented and primed during elution by adding 19.5 μ g of Elute, Prime, Fragment, High mix to the beads and incubating the samples for 8 min at 94°C. After fragmentation, 17 μ l of supernatant was removed from the beads and we proceeded immediately to synthesize first-strand cDNA.

Following the protocol, 8 μ l of first-strand synthesis mix Act D and SuperScript II mix (Illumina) was added to each sample, and the mixture was heated on a thermocycler using preprogrammed thermal conditions. Once the reaction finished and its temperature reached 4°C, we immediately proceeded to second-strand cDNA synthesis.

Diluted end repair control and second-strand marking mix were added, and the reaction mixture was mixed well and incubated in a preheated thermocycler at 16°C for 1 h. The DNA was purified using Agencourt AMPure XP beads (Beckman). Finally, samples were eluted with resuspension buffer and 15 μ l of elute was collected and stored at -20°C.

An A-Tailing control and an A-Tailing mix were added to the purified samples, and the samples were incubated on the preprogrammed thermal cycler. Once the incubation was done, we proceeded immediately to ligate adapters. Diluted ligation control, ligation mix, and barcodes were added, and the mixtures were incubated in a preheated thermocycler at 30°C for 10 min. Stop ligation buffer was immediately added to each sample, and the samples were mixed well. The ligated samples were then purified using Agencourt AMPure XP beads. We performed elutions with 50 μ l of resuspension buffer, and the elute was purified for a second time using Agencourt AMPure XP beads. Afterward, the final elution, consisting of 20 μ l of the elute, was collected and used for DNA enrichment. Samples were barcoded with Illumina TruSeq adapters as listed in Table S2. A complete list of the barcode sequences can be obtained from the Illumina support site (https://support.illumina.com/content/dam/illumina-support/documents/documentation/chemistry_documentation/experiment-design/illumina-adapter-sequences-100000002694-11.pdf).

PCR primer cocktail mix and PCR master mix were added to the samples, and the samples were incubated on a preprogrammed thermal cycler. The samples were then purified using Agencourt AMPure XP beads. Finally, 30 μ l of eluted library was collected and stored at -20°C.

Libraries were validated by quality, where size, purity, and semiquantitation determinations were performed using an Agilent Bioanalyzer and an Agilent DNA 1000 kit. The final fragment size for all the samples was approximately 300 bp, which is the expected size according to the protocol. Libraries were also validated by quantity. Sequencing library quantitation was performed by qPCR using a KAPA library quantitation kit (KAPA Biosystems) for Illumina Platforms. The standard curve method was used for quantitation with 1 to 5 of the DNA standards that came with the kit.

Ten microliters of sample was transferred from the wells to a new Midi plate. We then normalized the concentrations of the libraries to 10 nM using Tris-HCl (10 mM, pH 8.5)-0.1% Tween 20. Five microliters of each sample was then transferred to be pooled into a new LowBind 1.5-ml microcentrifuge tube for a total library volume of 60 μ l (pooled at 10 nM). Then, a 4 nM dilution was made from the 10 nM pooled library by dilution with Tris-HCl (10 mM, pH 8.5)-0.1% Tween 20.

A total volume of 1.3 ml of 1.8 pM denatured library is needed for sequencing using a v2 kit. A pooled 4 nM library was denatured by mixing with diluted NaOH and was incubated at room temperature for 5 min. Tris-HCl (200 mM, pH 7.0) was then added. The reaction mixture was diluted to 20 pM using a prechilled hybridization buffer. The 20 pM denatured library was further diluted to 1.8 pM using the same hybridization buffer. Before loading onto the reagent cartridge was performed, 1.3 μ l of denatured 20 pM Phix control was added to the 1,299 μ l of denatured 1.8 pM library to achieve a total volume of 1.3 ml for the sequencing run.

Sequencing was performed on an Illumina NextSeq 500 system at the University of Louisville Center for Genetics and Molecular Medicines (CGeMM) by the use of NextSeq 500/550 1 \times 75-cycle high-output kit v2.

RNAi knockdown. Human LARP7 small interfering RNA (siRNA) lentivector against four LARP7 target sequences and scrambled siRNA GFP lentivector were used with pLenti-P2A, pLenti-P2B, and Lentifectin to produce lentiviral particles per the protocol of the manufacturer (Applied Biological Materials, Inc.). Lentiviral particles were mixed with complete RPMI medium (Corning) containing 8 μ g/ml Polybrene (Millipore). The mixture of virus and medium was added to wells at 50 μ l mixture per 1 ml of cells and incubated for 24 h.

ankH cloning and protein expression. The *ankH* gene (Uniprot: Q5ZT65) from *Legionella pneumophila* strain Philadelphia 1 was cloned into vector pMCSG7, a derivative of vector pET-21a adapted for ligation-independent cloning (PMID: 18988021). This plasmid was then transformed into BL21(DE3) cells. The expressed protein contained a tobacco etch virus (TEV)-cleavable 6 \times His tag at the N terminus. For large-scale expression, a 15-ml overnight culture in LB was inoculated into 1 liter of Terrific broth medium (Bio Basic Inc., Markham, Ontario, Canada). The inoculated culture was grown at 37°C and was induced with 1 mM isopropyl β -D-1-thiogalactopyranoside when the optical density at 600 nm (OD_{600}) reached 0.6, and the temperature was reduced to 18°C for overnight growth. The cells were harvested by centrifugation at 9,000 \times g for 15 min.

For expression of the Se-methionine derivative, the cell pellet from 100 ml of overnight culture grown in LB media was inoculated into 1 liter of M9 minimal media. After shaking at 37°C was performed until the OD_{600} reached 0.6, a mixture of L-amino acids (100 mg of lysine, phenylalanine, and threonine; 50 mg of isoleucine, leucine, and valine) and 60 mg of Se-methionine was added to the culture. Protein expression was induced by adding 1 mM isopropyl β -D-1-thiogalactopyranoside after 15 min. The induced culture was grown overnight at 18°C, and the cells were harvested by centrifugation at 9,000 \times g for 15 min.

Protein purification. The cell pellet was resuspended in lysis buffer (50 mM Tris-HCl buffer [pH 8.0], 10% glycerol, 0.1% Triton X). The cells were lysed in a cell disruptor (Constant Systems Ltd.). The cell debris was removed by centrifugation at 31,000 \times g for 30 min. The resulting supernatant was applied to a 3 ml Talon cobalt metal-affinity column (Clontech). The column was washed with 5 column volumes of standard buffer (20 mM Tris [pH 8.0], 50 mM NaCl). A step gradient containing 100 mM and 200 mM imidazole in standard buffer was used to elute the His-tagged protein. Fractions containing AnkH were pooled and loaded on a Superdex 200 10/300 GL column (GE Healthcare) equilibrated with crystallization buffer (15 mM Tris-HCl [pH 8.0], 100 mM NaCl). AnkH-containing fractions were pooled and concentrated to 5 mg/ml in a Millipore centrifugal filter with a molecular weight cutoff of 10,000 Da for crystallization trials. The concentration was measured using a NanoDrop UV spectrophotometer (Thermo Scientific) and an extinction coefficient of 70,250 for AnkH, calculated by the use of the ProtParam tool (100).

Protein crystallization and data collection. Initial crystals were obtained by screening and were optimized using the 24-well plate format. The best crystals were obtained by the hanging-drop method by mixing 1 μ l of protein solution and 1 μ l of reservoir solution containing 1.0 M ammonium tartrate dibasic (pH 7.0). The drop was incubated over a 0.5-ml reservoir solution. The crystals were cryoprotected in solution containing 70% of reservoir solution and 30% glycerol. Crystals were flash cooled in liquid nitrogen, and diffraction data were collected at the 08ID and 08BM beamlines at the Canadian Light Source. Data were processed and scaled with XDS. The same procedure was followed for the Se-methionine-labeled derivative.

Structure determination. The native and SeMet data set were indexed, integrated, and scaled using Program HKL3000 (101). Experimental phases were obtained by the single-wavelength anomalous dispersion (SAD) method, and the structure was solved using Program HKL3000. The autobuilt model from HKL3000 was \sim 90% complete, and the remaining 10% of the molecule was built manually using Coot software (PMID: 20383002). The refinement was done using the Phenix program suite (102). The model contained residues 1 to 461 and was refined to $R_{work} = 0.172$ and $R_{free} = 0.210$. The geometry was validated with the program MolProbity (103). The pertinent details of data collection and refinement are listed in Table S5. The coordinates and structure factors were deposited with the Protein Data Bank with the code 6MCA. The crystal structure was modeled using Chimera software (University of California, San Francisco [UCSF]), and structure similarity to other peptidases was determined using the MEROPS peptidase database (89).

Statistical analysis. All experiments were performed using at least three independent biological repeats, and the data shown are representative of results from one experiment. To analyze for statistically significant differences among three sets of data, the two-tailed Student's *t* test was used, and the *P* value was obtained.

Data availability. Atomic coordinates and diffraction data for the structure have been deposited with PDB (<https://www.rcsb.org/>) under PDB ID 6MCA. The RNA-Seq data have been submitted to the GEO database (<https://www.ncbi.nlm.nih.gov/geo/>), accession no. GSE135803.

SUPPLEMENTAL MATERIAL

Supplemental material for this article may be found at <https://doi.org/10.1128/mBio.01942-19>.

TABLE S1, DOCX file, 0.02 MB.

TABLE S2, DOCX file, 0.02 MB.

TABLE S3, DOCX file, 0.02 MB.

TABLE S4, DOCX file, 0.1 MB.

TABLE S5, DOCX file, 0.02 MB.

ACKNOWLEDGMENTS

Y.A.K. is supported by Public Health Service Awards R01AI120244 and R01AI140195 from the NIAID and by the Commonwealth of Kentucky Research Challenge Trust Fund.

The M.C. laboratory is supported by Canadian Institutes of Health Research grant MOP 48370. The X-ray data were collected at the Canadian Light Source, which is supported by the Canada Foundation for Innovation, Natural Sciences and Engineering Research Council of Canada, the University of Saskatchewan, the Government of Saskatchewan, Western Economic Diversification Canada, the National Research Council Canada, and the Canadian Institutes of Health Research.

J.V.D., I.C., C.P., M.C., and Y.A.K. conceived the study; J.V.D., I.C., and L.L. performed experiments; J.V.D., I.C., L.L., M.C., and Y.A.K. analyzed the data; and J.V.D., I.C., M.C., and Y.A.K. wrote and revised the manuscript. All of us read and approved the final manuscript.

Part of this work was performed with assistance of the UofL Genomics Facility, which is supported by NIH P20GM103436 (KY IDeA Networks of Biomedical Research Excellence), the J. G. Brown Cancer Center, and user fees. We declare that we have no competing interests.

REFERENCES

1. Abu Khweek A, Amer AO. 2018. Factors mediating environmental biofilm formation by *Legionella pneumophila*. *Front Cell Infect Microbiol* 8:38. <https://doi.org/10.3389/fcimb.2018.00038>.
2. Fields BS. 1996. The molecular ecology of legionellae. *Trends Microbiol* 4:286–290. [https://doi.org/10.1016/0966-842X\(96\)10041-X](https://doi.org/10.1016/0966-842X(96)10041-X).
3. Horwitz MA, Silverstein SC. 1980. Legionnaires' disease bacterium (*Legionella pneumophila*) multiplies intracellularly in human monocytes. *J Clin Invest* 66:441–450. <https://doi.org/10.1172/JCI109874>.
4. Rowbotham TJ. 1980. Preliminary report on the pathogenicity of *Legionella pneumophila* for freshwater and soil amoebae. *J Clin Pathol* 33:1179–1183. <https://doi.org/10.1136/jcp.33.12.1179>.
5. Swart AL, Harrison CF, Eichinger L, Steinert M, Hilbi H. 2018. Acanthamoeba and dictyostelium as cellular models for Legionella infection. *Front Cell Infect Microbiol* 8:61. <https://doi.org/10.3389/fcimb.2018.00061>.
6. Abu Kwaik Y, Gao L-Y, Stone BJ, Venkataraman C, Harb OS. 1998. Invasion of protozoa by *Legionella pneumophila* and its role in bacterial ecology and pathogenesis. *Appl Environ Microbiol* 64:3127–3133.
7. Fields BS, Benson RF, Besser RE. 2002. Legionella and Legionnaires' disease: 25 years of investigation. *Clin Microbiol Rev* 15:506–526. <https://doi.org/10.1128/cmr.15.3.506-526.2002>.
8. Garcia MT, Jones S, Pelaz C, Millar RD, Abu Kwaik Y. 2007. Acanthamoeba polyphaga resuscitates viable non-culturable Legionella pneumophila after disinfection. *Environ Microbiol* 9:1267–1277. <https://doi.org/10.1111/j.1462-2920.2007.01245.x>.
9. Best AM, Abu Kwaik Y. 2019. Evasion of phagotrophic predation by protist hosts and innate immunity of metazoan hosts by Legionella pneumophila. *Cell Microbiol* 21:e12971. <https://doi.org/10.1111/cmi.12971>.
10. Boamah DK, Zhou G, Ensminger AW, O'Connor TJ. 2017. From many hosts, one accidental pathogen: the diverse protozoan hosts of Legionella. *Front Cell Infect Microbiol* 7:477. <https://doi.org/10.3389/fcimb.2017.00477>.
11. Wu H-Y, Yan H, Zheng M-L, Sun M-M, Wang Q, Hu C-M, Zhan X-Y, Yuan M-G, Qu P-H, Hu C-H. 2019. Legionella qingyii sp. nov., isolated from water samples in China. *Int J Syst Evol Microbiol* 69:2017–2022. <https://doi.org/10.1099/ijsem.0.003421>.
12. Burstein D, Amaro F, Zusman T, Lifshitz Z, Cohen O, Gilbert JA, Pupko T, Shuman HA, Segal G. 2016. Genomic analysis of 38 Legionella species identifies large and diverse effector repertoires. *Nat Genet* 48:167–175. <https://doi.org/10.1038/ng.3481>.
13. Gomez-Valero L, Rusniok C, Rolando M, Neou M, Dervins-Ravault D, Demirtas J, Rouy Z, Moore RJ, Chen H, Petty NK, Jarraud S, Etienne J, Steinert M, Heuner K, Gribaldo S, Médigue C, Glöckner G, Hartland EL, Buchrieser C. 2014. Comparative analyses of Legionella species identifies genetic features of strains causing Legionnaires' disease. *Genome Biol* 15:505. <https://doi.org/10.1186/PREACCEPT-1086350395137407>.
14. Gomez-Valero L, Rusniok C, Carson D, Mondino S, Pérez-Cobas AE, Rolando M, Pasricha S, Reuter S, Demirtas J, Crumbach J, Descorps-Declere S, Hartland EL, Jarraud S, Dougan G, Schroeder GN, Frankel G, Buchrieser C. 2019. More than 18,000 effectors in the Legionella genus genome provide multiple, independent combinations for replication in human cells. *Proc Natl Acad Sci U S A* 116:2265–2273. <https://doi.org/10.1073/pnas.1808016116>.
15. Yu VL, Plouffe JF, Pastoris MC, Stout JE, Schousboe M, Widmer A, Summersgill J, File T, Heath CM, Paterson DL, Cheresky A. 2002. Distribution of Legionella species and serogroups isolated by culture in patients with sporadic community-acquired legionellosis: an international collaborative survey. *J Infect Dis* 186:127–128. <https://doi.org/10.1086/341087>.
16. Isberg RR, O'Connor TJ, Heidtman M. 2009. The Legionella pneumophila replication vacuole: making a cozy niche inside host cells. *Nat Rev Microbiol* 7:13–24. <https://doi.org/10.1038/nrmicro1967>.
17. Luo ZQ. 2011. Legionella secreted effectors and innate immune responses. *Cell Microbiol* <https://doi.org/10.1111/j.1462-5822.2011.01713.x>.
18. Molmeret M, Horn M, Wagner M, Santic M, Abu Kwaik Y. 2005. Amoebae as training grounds for intracellular bacterial pathogens. *Appl Environ Microbiol* 71:20–28. <https://doi.org/10.1128/AEM.71.1.20-28.2005>.
19. Oliva G, Sahr T, Buchrieser C. 2018. The life cycle of *L. pneumophila*: cellular differentiation is linked to virulence and metabolism. *Front Cell Infect Microbiol* 8:3. <https://doi.org/10.3389/fcimb.2018.00003>.

20. Shin S, Roy CR. 2008. Host cell processes that influence the intracellular survival of *Legionella pneumophila*. *Cell Microbiol* 10:1209–1220. <https://doi.org/10.1111/j.1462-5822.2008.01145.x>.
21. Coers J, Monahan C, Roy CR. 1999. Modulation of phagosome biogenesis by *Legionella pneumophila* creates an organelle permissive for intracellular growth. *Nat Cell Biol* 1:451–453. <https://doi.org/10.1038/15687>.
22. Kagan JC, Roy CR. 2002. *Legionella* phagosomes intercept vesicular traffic from endoplasmic reticulum exit sites. *Nat Cell Biol* 4:945–954. <https://doi.org/10.1038/ncb883>.
23. Barlocher K, Welin A, Hilbi H. 2017. Formation of the *Legionella* replicative compartment at the crossroads of retrograde trafficking. *Front Cell Infect Microbiol* 7:482. <https://doi.org/10.3389/fcimb.2017.00482>.
24. Ghosh S, O'Connor TJ. 2017. Beyond paralogs: the multiple layers of redundancy in bacterial pathogenesis. *Front Cell Infect Microbiol* 7:467. <https://doi.org/10.3389/fcimb.2017.00467>.
25. Steiner B, Swart AL, Welin A, Weber S, Personnic N, Kaech A, Freyre C, Ziegler U, Klemm RW, Hilbi H. 2017. ER remodeling by the large GTPase atlastin promotes vacuolar growth of *Legionella pneumophila*. *EMBO Rep* 18:1817. <https://doi.org/10.15252/embr.201743903>.
26. Ensminger AW. 2016. *Legionella pneumophila*, armed to the hilt: justifying the largest arsenal of effectors in the bacterial world. *Curr Opin Microbiol* 29:74–80. <https://doi.org/10.1016/j.mib.2015.11.002>.
27. Schroeder GN. 2018. The toolbox for uncovering the functions of *Legionella* Dot/Icm type IVb secretion system effectors: current state and future directions. *Front Cell Infect Microbiol* 7:528. <https://doi.org/10.3389/fcimb.2017.00528>.
28. Manske C, Hilbi H. 2014. Metabolism of the vacuolar pathogen *Legionella* and implications for virulence. *Front Cell Infect Microbiol* 4:125. <https://doi.org/10.3389/fcimb.2014.00125>.
29. Qiu J, Luo Z-Q. 2017. *Legionella* and *Coxiella* effectors: strength in diversity and activity. *Nat Rev Microbiol* 15:591–605. <https://doi.org/10.1038/nrmicro.2017.67>.
30. Qiu J, Luo Z-Q. 2017. Hijacking of the host ubiquitin network by *Legionella pneumophila*. *Front Cell Infect Microbiol* 7:487. <https://doi.org/10.3389/fcimb.2017.00487>.
31. O'Connor TJ, Adepoju Y, Boyd D, Isberg RR. 2011. Minimization of the *Legionella pneumophila* genome reveals chromosomal regions involved in host range expansion. *Proc Natl Acad Sci U S A* 108:14733–14740. <https://doi.org/10.1073/pnas.1111678108>.
32. Best A, Abu Kwaik Y. 2018. Evolution of the arsenal of *Legionella pneumophila* effectors to modulate protist hosts. *mBio* 9:e01313-18. <https://doi.org/10.1128/mBio.01313-18>.
33. Al-Quadan T, Price C, Abu Kwaik Y. 2012. Exploitation of evolutionarily conserved amoeba and mammalian processes by *Legionella*. *Trends Microbiol* 20:299–306. <https://doi.org/10.1016/j.tim.2012.03.005>.
34. Cazalet C, Rusniok C, Bruggemann H, Zidane N, Magnier A, Ma L, Tichit M, Jarraud S, Bouchier C, Vandenesch F, Kunst F, Etienne J, Glaser P, Buchrieser C. 2004. Evidence in the *Legionella pneumophila* genome for exploitation of host cell functions and high genome plasticity. *Nat Genet* 36:1165–1173. <https://doi.org/10.1038/ng1447>.
35. de Felipe KS, Pampou S, Jovanovic OS, Pericone CD, Ye SF, Kalachikov S, Shuman HA. 2005. Evidence for acquisition of *Legionella* type IV secretion substrates via interdomain horizontal gene transfer. *J Bacteriol* 187:7716–7726. <https://doi.org/10.1128/JB.187.22.7716-7726.2005>.
36. Franco IS, Shuman HA, Charpentier X. 2009. The perplexing functions and surprising origins of *Legionella pneumophila* type IV secretion effectors. *Cell Microbiol* 11:1435–1443. <https://doi.org/10.1111/j.1462-5822.2009.01351.x>.
37. Gomez-Valero L, Rusniok C, Cazalet C, Buchrieser C. 2011. Comparative and functional genomics of *Legionella* identified eukaryotic like proteins as key players in host-pathogen interactions. *Front Microbiol* 2:208. <https://doi.org/10.3389/fmicb.2011.00208>.
38. Al-Khodor S, Price CT, Habyarimana F, Kalia A, Abu Kwaik Y. 2008. A Dot/Icm-translocated ankyrin protein of *Legionella pneumophila* is required for intracellular proliferation within human macrophages and protozoa. *Mol Microbiol* 70:908–923. <https://doi.org/10.1111/j.1365-2958.2008.06453.x>.
39. Ivanov SS, Charron G, Hang HC, Roy CR. 2010. Lipidation by the host prenyltransferase machinery facilitates membrane localization of *Legionella pneumophila* effector proteins. *J Biol Chem* 285:34686–34698. <https://doi.org/10.1074/jbc.M110.170746>.
40. Kubori T, Hyakutake A, Nagai H. 2008. *Legionella* translocates an E3 ubiquitin ligase that has multiple U-boxes with distinct functions. *Mol Microbiol* 67:1307–1319. <https://doi.org/10.1111/j.1365-2958.2008.06124.x>.
41. Price CT, Al-Khodor S, Al-Quadan T, Santic M, Habyarimana F, Kalia A, Kwaik YA. 2009. Molecular mimicry by an F-box effector of *Legionella pneumophila* hijacks a conserved polyubiquitination machinery within macrophages and protozoa. *PLoS Pathog* 5:e1000704. <https://doi.org/10.1371/journal.ppat.1000704>.
42. Zamboni DS, Kobayashi KS, Holsdorf T, Ogura Y, Long EM, Vance RE, Kuida K, Mariathasan S, Dixit VM, Flavell RA, Dietrich WF, Roy CR. 2006. The Birc1e cytosolic pattern-recognition receptor contributes to the detection and control of *Legionella pneumophila* infection. *Nat Immunol* 7:318–325. <https://doi.org/10.1038/ni1305>.
43. Binz HK, Kohl A, Pluckthun A, Grutter MG. 2006. Crystal structure of a consensus-designed ankyrin repeat protein: implications for stability. *Proteins* 65:280–284. <https://doi.org/10.1002/prot.20930>.
44. Bork P. 1993. Hundreds of ankyrin-like repeats in functionally diverse proteins: mobile modules that cross phyla horizontally? *Proteins* 17:363–374. <https://doi.org/10.1002/prot.340170405>.
45. Kohl A, Binz HK, Forrer P, Stump MT, Pluckthun A, Grutter MG. 2003. Designed to be stable: crystal structure of a consensus ankyrin repeat protein. *Proc Natl Acad Sci U S A* 100:1700–1705. <https://doi.org/10.1073/pnas.0337680100>.
46. Li J, Mahajan A, Tsai MD. 2006. Ankyrin repeat: a unique motif mediating protein-protein interactions. *Biochemistry* 45:15168–15178. <https://doi.org/10.1021/bi062188q>.
47. Mosavi LK, Minor DL, Jr, Peng ZY. 2002. Consensus-derived structural determinants of the ankyrin repeat motif. *Proc Natl Acad Sci U S A* 99:16029–16034. <https://doi.org/10.1073/pnas.252537899>.
48. Yu H, Kohl A, Binz HK, Pluckthun A, Grutter MG, van Gunsteren WF. 2006. Molecular dynamics study of the stabilities of consensus designed ankyrin repeat proteins. *Proteins* 65:285–295. <https://doi.org/10.1002/prot.20991>.
49. Sedgwick SG, Smerdon SJ. 1999. The ankyrin repeat: a diversity of interactions on a common structural framework. *Trends Biochem Sci* 24:311–316. [https://doi.org/10.1016/S0968-0004\(99\)01426-7](https://doi.org/10.1016/S0968-0004(99)01426-7).
50. Islam Z, Nagampalli RSK, Fatima MT, Ashraf GM. 2018. New paradigm in ankyrin repeats: beyond protein-protein interaction module. *Int J Biol Macromol* 109:1164–1173. <https://doi.org/10.1016/j.ijbiomac.2017.11.101>.
51. Al-Khodor S, Price CT, Kalia A, Abu Kwaik Y. 2010. Functional diversity of ankyrin repeats in microbial proteins. *Trends Microbiol* 18:132–139. <https://doi.org/10.1016/j.tim.2009.11.004>.
52. Pan X, Luhrmann A, Satoh A, Laskowski-Arce MA, Roy CR. 2008. Ankyrin repeat proteins comprise a diverse family of bacterial type IV effectors. *Science* 320:1651–1654. <https://doi.org/10.1126/science.1158160>.
53. Habyarimana F, Al-Khodor S, Kalia A, Graham JE, Price CT, Garcia MT, Kwaik YA. 2008. Role for the ankyrin eukaryotic-like genes of *Legionella pneumophila* in parasitism of protozoan hosts and human macrophages. *Environ Microbiol* 10:1460–1474. <https://doi.org/10.1111/j.1462-2920.2007.01560.x>.
54. Habyarimana F, Price CT, Santic M, Al-Khodor S, Kwaik YA. 2010. Molecular characterization of the Dot/Icm-translocated AnkH and AnkJ eukaryotic-like effectors of *Legionella pneumophila*. *Infect Immun* 78:1123–1134. <https://doi.org/10.1128/IAI.00913-09>.
55. Price C, Merchant M, Jones S, Best A, Von Dwingelo J, Lawrenz MB, Alam N, Schueler-Furman O, Kwaik YA. 2017. Host FIH-mediated asparaginyl hydroxylation of translocated *Legionella pneumophila* effectors. *Front Cell Infect Microbiol* 7:54. <https://doi.org/10.3389/fcimb.2017.00054>.
56. Belyi Y, Niggeweg R, Opitz B, Vogelsgesang M, Hippenstiel S, Wilm M, Aktories K. 2006. *Legionella pneumophila* glucosyltransferase inhibits host elongation factor 1A. *Proc Natl Acad Sci U S A* 103:16953–16958. <https://doi.org/10.1073/pnas.0601562103>.
57. Belyi Y, Tabakova I, Stahl M, Aktories K. 2008. Lgt: a family of cytotoxic glucosyltransferases produced by *Legionella pneumophila*. *J Bacteriol* 190:3026–3035. <https://doi.org/10.1128/JB.01798-07>.
58. Fontana MF, Banga S, Barry KC, Shen X, Tan Y, Luo ZQ, Vance RE. 2011. Secreted bacterial effectors that inhibit host protein synthesis are critical for induction of the innate immune response to virulent *Legionella pneumophila*. *PLoS Pathog* 7:e1001289. <https://doi.org/10.1371/journal.ppat.1001289>.
59. Shen X, Banga S, Liu Y, Xu L, Gao P, Shamovsky I, Nudler E, Luo ZQ. 2009. Targeting eEF1A by a *Legionella pneumophila* effector leads to inhibition of protein synthesis and induction of host stress response. *Cell Microbiol* 11:911–926. <https://doi.org/10.1111/j.1462-5822.2009.01301.x>.

60. Li T, Lu Q, Wang G, Xu H, Huang H, Cai T, Kan B, Ge J, Shao F. 2013. SET-domain bacterial effectors target heterochromatin protein 1 to activate host rDNA transcription. *EMBO Rep* 14:733–740. <https://doi.org/10.1038/embor.2013.86>.
61. Rolando M, Sanulli S, Rusniok C, Gomez-Valero L, Bertholet C, Sahr T, Margueron R, Buchrieser C. 2013. Legionella pneumophila effector RomA uniquely modifies host chromatin to repress gene expression and promote intracellular bacterial replication. *Cell Host Microbe* 13:395–405. <https://doi.org/10.1016/j.chom.2013.03.004>.
62. Lee PC, Machner MP. 2018. The Legionella effector kinase LegK7 hijacks the host Hippo pathway to promote infection. *Cell Host Microbe* 24:429–438.e6. <https://doi.org/10.1016/j.chom.2018.08.004>.
63. Price DH. 2000. P-TEFb, a cyclin-dependent kinase controlling elongation by RNA polymerase II. *Mol Cell Biol* 20:2629–2634. <https://doi.org/10.1128/mcb.20.8.2629-2634.2000>.
64. Zhou Q, Li T, Price DH. 2012. RNA polymerase II elongation control. *Annu Rev Biochem* 81:119–143. <https://doi.org/10.1146/annurev-biochem-052610-095910>.
65. Uchikawa E, Natchiar KS, Han X, Proux F, Roblin P, Zhang E, Durand A, Klaholz BP, Dock-Bregeon AC. 2015. Structural insight into the mechanism of stabilization of the 7SK small nuclear RNA by LARP7. *Nucleic Acids Res* 43:3373–3388. <https://doi.org/10.1093/nar/gkv173>.
66. Barboric M, Lenasi T, Chen H, Johansen EB, Guo S, Peterlin BM. 2009. 7SK snRNP/P-TEFb couples transcription elongation with alternative splicing and is essential for vertebrate development. *Proc Natl Acad Sci U S A* 106:7798–7803. <https://doi.org/10.1073/pnas.0903188106>.
67. He N, Jahchan NS, Hong E, Li Q, Bayfield MA, Maraja RJ, Luo K, Zhou Q. 2008. A La-related protein modulates 7SK snRNP integrity to suppress P-TEFb-dependent transcriptional elongation and tumorigenesis. *Mol Cell* 29:588–599. <https://doi.org/10.1016/j.molcel.2008.01.003>.
68. Muniz L, Egloff S, Kiss T. 2013. RNA elements directing in vivo assembly of the 7SK/MePCE/Larp7 transcriptional regulatory snRNP. *Nucleic Acids Res* 41:4686–4698. <https://doi.org/10.1093/nar/gkt159>.
69. Xue Y, Yang Z, Chen R, Zhou Q. 2010. A capping-independent function of MePCE in stabilizing 7SK snRNA and facilitating the assembly of 7SK snRNP. *Nucleic Acids Res* 38:360–369. <https://doi.org/10.1093/nar/gkp977>.
70. Guo J, Price DH. 2013. RNA polymerase II transcription elongation control. *Chem Rev* 113:8583–8603. <https://doi.org/10.1021/cr400105n>.
71. Jeronimo C, Forget D, Bouchard A, Li Q, Chua G, Poitras C, Therien C, Bergeron D, Bourassa S, Greenblatt J, Chabot B, Poirier GG, Hughes TR, Blanchette M, Price DH, Coulombe B. 2007. Systematic analysis of the protein interaction network for the human transcription machinery reveals the identity of the 7SK capping enzyme. *Mol Cell* 27:262–274. <https://doi.org/10.1016/j.molcel.2007.06.027>.
72. Michels AA, Fraldi A, Li Q, Adamson TE, Bonnet F, Nguyen VT, Sedore SC, Price JP, Price DH, Lania L, Bensaude O. 2004. Binding of the 7SK snRNA turns the HEXIM1 protein into a P-TEFb (CDK9/cyclin T) inhibitor. *EMBO J* 23:2608–2619. <https://doi.org/10.1038/sj.emboj.7600275>.
73. Yik JH, Chen R, Nishimura R, Jennings JL, Link AJ, Zhou Q. 2003. Inhibition of P-TEFb (CDK9/cyclin T) kinase and RNA polymerase II transcription by the coordinated actions of HEXIM1 and 7SK snRNA. *Mol Cell* 12:971–982. [https://doi.org/10.1016/S1097-2765\(03\)00388-5](https://doi.org/10.1016/S1097-2765(03)00388-5).
74. Nguyen VT, Kiss T, Michels AA, Bensaude O. 2001. 7SK small nuclear RNA binds to and inhibits the activity of CDK9/cyclin T complexes. *Nature* 414:322–325. <https://doi.org/10.1038/35104581>.
75. Yang Z, Zhu Q, Luo K, Zhou Q. 2001. The 7SK small nuclear RNA inhibits the CDK9/cyclin T1 kinase to control transcription. *Nature* 414:317–322. <https://doi.org/10.1038/35104575>.
76. Perumal K, Sinha K, Henning D, Reddy R. 2001. Purification, characterization, and cloning of the cDNA of human signal recognition particle RNA 3'-adenylating enzyme. *J Biol Chem* 276:21791–21796. <https://doi.org/10.1074/jbc.M101905200>.
77. Sinha KM, Gu J, Chen Y, Reddy R. 1998. Adenylation of small RNAs in human cells. Development of a cell-free system for accurate adenylation on the 3'-end of human signal recognition particle RNA. *J Biol Chem* 273:6853–6859. <https://doi.org/10.1074/jbc.273.12.6853>.
78. Peterlin BM, Price DH. 2006. Controlling the elongation phase of transcription with P-TEFb. *Mol Cell* 23:297–305. <https://doi.org/10.1016/j.molcel.2006.06.014>.
79. Price CT, Al-Quadan T, Santic M, Jones SC, Abu Kwaik Y. 2010. Exploitation of conserved eukaryotic host cell farnesylation machinery by an F-box effector of Legionella pneumophila. *J Exp Med* 207:1713–1726. <https://doi.org/10.1084/jem.20100771>.
80. Krueger BJ, Jeronimo C, Roy BB, Bouchard A, Barrandon C, Byers SA, Searcey CE, Cooper JJ, Bensaude O, Cohen EA, Coulombe B, Price DH. 2008. LARP7 is a stable component of the 7SK snRNP while P-TEFb, HEXIM1 and hnRNP A1 are reversibly associated. *Nucleic Acids Res* 36:2219–2229. <https://doi.org/10.1093/nar/gkn061>.
81. Holm L, Rosenstrom P. 2010. Dali server: conservation mapping in 3D. *Nucleic Acids Res* 38:W545–W549. <https://doi.org/10.1093/nar/gkq366>.
82. Abendroth U, Adlung N, Otto A, Gruneisen B, Becher D, Bonas U. 2017. Identification of new protein-coding genes with a potential role in the virulence of the plant pathogen Xanthomonas euvesicatoria. *BMC Genomics* 18:625. <https://doi.org/10.1186/s12864-017-4041-7>.
83. Chosed R, Tomchick DR, Brautigam CA, Mukherjee S, Negi VS, Machius M, Orth K. 2007. Structural analysis of Xanthomonas XopD provides insights into substrate specificity of ubiquitin-like protein proteases. *J Biol Chem* 282:6773–6782. <https://doi.org/10.1074/jbc.M608730200>.
84. Pruneda JN, Durkin CH, Geurink PP, Ovaa H, Santhanam B, Holden DW, Komander D. 2016. The molecular basis for ubiquitin and ubiquitin-like specificities in bacterial effector proteases. *Mol Cell* 63:261–276. <https://doi.org/10.1016/j.molcel.2016.06.015>.
85. Yang A, Pantoom S, Wu YW. 2017. Elucidation of the anti-autophagy mechanism of the Legionella effector RavZ using semisynthetic LC3 proteins. *Elife* 6:e23905. <https://doi.org/10.7554/eLife.23905>.
86. Horenkamp FA, Kauffman KJ, Kohler LJ, Sherwood RK, Krueger KP, Shteyn V, Roy CR, Melia TJ, Reinisch KM. 2015. The Legionella anti-autophagy effector RavZ targets the autophagosome via PI3P- and curvature-sensing motifs. *Dev Cell* 34:569–576. <https://doi.org/10.1016/j.devcel.2015.08.010>.
87. Finn RD, Attwood TK, Babbitt PC, Bateman A, Bork P, Bridge AJ, Chang HY, Dosztanyi Z, El-Gebali S, Fraser M, Gough J, Haft D, Holliday GL, Huang H, Huang X, Letunic I, Lopez R, Lu S, Marchler-Bauer A, Mi H, Mistry J, Natale DA, Necci M, Nuka G, Orengo CA, Park Y, Pesseat S, Piovesan D, Potter SC, Rawlings ND, Redaschi N, Richardson L, Rivoire C, Sangrador-Vegas A, Sigrist C, Sillitoe A, Smithers B, Squizzato S, Sutton G, Thanki N, Thomas PD, Tosatto SC, Wu CH, Xenarios I, Yeh LS, Young SY, Mitchell AL. 2017. InterPro in 2017—beyond protein family and domain annotations. *Nucleic Acids Res* 45:D190–D199. <https://doi.org/10.1093/nar/gkw1107>.
88. Rawlings ND, Barrett AJ, Finn R. 2016. Twenty years of the MEROPS database of proteolytic enzymes, their substrates and inhibitors. *Nucleic Acids Res* 44:D343–D350. <https://doi.org/10.1093/nar/gkv1118>.
89. Rawlings ND, Barrett AJ, Thomas PD, Huang X, Bateman A, Finn RD. 2018. The MEROPS database of proteolytic enzymes, their substrates and inhibitors in 2017 and a comparison with peptidases in the PANTHER database. *Nucleic Acids Res* 46:D624–D632. <https://doi.org/10.1093/nar/gkx1134>.
90. Du Toit A. 2019. The effector repertoire of Legionella. *Nat Rev Microbiol* 17:126. <https://doi.org/10.1038/s41579-019-0155-z>.
91. Altschul SF, Madden TL, Schaffer AA, Zhang J, Zhang Z, Miller W, Lipman DJ. 1997. Gapped BLAST and PSI-BLAST: a new generation of protein database search programs. *Nucleic Acids Res* 25:3389–3402. <https://doi.org/10.1093/nar/25.17.3389>.
92. Mosavi LK, Cammett TJ, Desrosiers DC, Peng ZY. 2004. The ankyrin repeat as molecular architecture for protein recognition. *Protein Sci* 13:1435–1448. <https://doi.org/10.1110/ps.03554604>.
93. Lando D, Peet DJ, Whelan DA, Gorman JJ, Whitelaw ML. 2002. Asparagine hydroxylation of the HIF transactivation domain a hypoxic switch. *Science* 295:858–861. <https://doi.org/10.1126/science.1068592>.
94. Mahon PC, Hirota K, Semenza GL. 2001. FIH-1: a novel protein that interacts with HIF-1 α and VHL to mediate repression of HIF-1 transcriptional activity. *Genes Dev* 15:2675–2686. <https://doi.org/10.1101/gad.924501>.
95. Hewitson KS, McNeill LA, Riordan MV, Tian YM, Bullock AN, Welford RW, Elkins JM, Oldham NJ, Bhattacharya S, Gleadle JM, Ratcliffe PJ, Pugh CW, Schofield CJ. 2002. Hypoxia-inducible factor (HIF) asparagine hydroxylase is identical to factor inhibiting HIF (FIH) and is related to the cupin structural family. *J Biol Chem* 277:26351–26355. <https://doi.org/10.1074/jbc.C200273200>.
96. Yang M, Ge W, Chowdhury R, Claridge TD, Kramer HB, Schmierer B, McDonough MA, Gong L, Kessler BM, Ratcliffe PJ, Coleman ML, Schofield CJ. 2011. Asparagine and aspartate hydroxylation of the cytoskeletal ankyrin family is catalyzed by factor-inhibiting hypoxia-inducible factor. *J Biol Chem* 286:7648–7660. <https://doi.org/10.1074/jbc.M110.193540>.
97. Coleman ML, McDonough MA, Hewitson KS, Coles C, Mecinovic J, Edelmann M, Cook KM, Cockman ME, Lancaster DE, Kessler BM, Oldham NJ,

- Ratcliffe PJ, Schofield CJ. 2007. Asparaginyl hydroxylation of the Notch ankyrin repeat domain by factor inhibiting hypoxia-inducible factor. *J Biol Chem* 282:24027–24038. <https://doi.org/10.1074/jbc.M704102200>.
98. Stone BJ, Abu Kwaik Y. 1998. Expression of multiple pili by *Legionella pneumophila*: identification and characterization of a type IV pilin gene and its role in adherence to mammalian and protozoan cells. *Infect Immun* 66:1768–1775.
99. Bruckert WM, Abu Kwaik Y. 2016. Lysine11-linked polyubiquitination of the AnkB F-box effector of *Legionella pneumophila*. *Infect Immun* 84:99–107. <https://doi.org/10.1128/IAI.01165-15>.
100. Wilkins MR, Gasteiger E, Bairoch A, Sanchez JC, Williams KL, Appel RD, Hochstrasser DF. 1999. Protein identification and analysis tools in the ExPASy server. *Methods Mol Biol* 112:531–552.
101. Minor W, Cymborowski M, Otwinowski Z, Chruszcz M. 2006. HKL-3000: the integration of data reduction and structure solution—from diffraction images to an initial model in minutes. *Acta Crystallogr D Biol Crystallogr* 62:859–866. <https://doi.org/10.1107/S0907444906019949>.
102. Adams PD, Afonine PV, Bunkoczi G, Chen VB, Davis IW, Echols N, Headd JJ, Hung LW, Kapral GJ, Grosse-Kunstleve RW, McCoy AJ, Moriarty NW, Oeffner R, Read RJ, Richardson DC, Richardson JS, Terwilliger TC, Zwart PH. 2010. PHENIX: a comprehensive Python-based system for macromolecular structure solution. *Acta Crystallogr D Biol Crystallogr* 66: 213–221. <https://doi.org/10.1107/S0907444909052925>.
103. Chen VB, Arendall WB, III, Headd JJ, Keedy DA, Immormino RM, Kapral GJ, Murray LW, Richardson JS, Richardson DC. 2010. MolProbity: all-atom structure validation for macromolecular crystallography. *Acta Crystallogr D Biol Crystallogr* 66:12–21. <https://doi.org/10.1107/S0907444909042073>.